Hole superconductivity and the high-T_c oxides

F. Marsiglio and J. E. Hirsch

Department of Physics, University of California, San Diego, La Jolla, California 92093
(Received 12 October 1989)

We discuss predictions of the hole-pairing mechanism of superconductivity for various experimentally measurable properties of the high-T_c oxides. The model considered describes conduction by holes through the oxygen anion network in the high-T_c oxides, and pairing originates in a term in the Hamiltonian describing an enhanced hopping amplitude for a hole in the presence of other holes. The model includes on-site and nearest-neighbor Coulomb repulsions and different hopping amplitudes within and between planes. We use information from experiments to determine suitable ranges of parameters in the model and examine various properties of the superconducting state within this model using BCS theory. Among the most notable predictions of the model for the high-T_c oxides are: (1) the superconducting state is nearly isotropic despite the anisotropic band structure; (2) the pressure dependence of T_c is very different for pressure applied perpendicular and parallel to the planes; and (3) the upper critical field and effective mass decrease rapidly and monotonically with hole doping, as a crossover occurs between strong- and weak-coupling regimes.

I. INTRODUCTION

Various experimental measurements[1] indicate that the pairing formalism utilized by BCS theory is applicable to the high-T_c oxides, but there is still no consensus on the issue of what the "glue" is that is causing the pairing. One of us has proposed recently[2] that holes are the key component of superconductivity, and in particular that in high-T_c oxides superconductivity originates from conduction of holes through O^{2-} anions. The reason that holes conducting through closed-shell anions give rise to high-temperature superconductivity can be understood in two ways: (a) a hole causes a large disruption of its background, the filled-shell anion, which can be described by coupling of the hole to a pseudospin degree of freedom located at the anion site, and a second hole can take advantage of this distorted background,[2] or (b) an off-diagonal matrix element of the Coulomb interaction is attractive when the single-particle wave function changes sign between a site and its nearest neighbor, which occurs for holes in a filled band.[3] These two points of view are equivalent and lead to an identical conclusion, a term in the Hamiltonian describing an enhanced hopping rate for a hole if other holes are in the nearby vicinity. This term explicitly breaks electron-hole symmetry and, together with an attractive interaction between holes, it causes considerable effective-mass enhancement for nearly filled electron bands.[3]

Many of the consequences of such a Hamiltonian have already been worked out in a BCS framework.[4] In this paper we focus on parameter regimes that may be specifically applicable to high-T_c oxides, and, in addition, we include the following elements that were left out in our previous discussion of the oxides.[4] (a) We examine the effect of a nearest neighbor Coulomb repulsion V in addition to the on-site repulsion U. While this interaction is probably small in the oxides, it is important to

determine how robust the superconducting state is to the inclusion of such a term and what quantitative or qualitative changes it can cause in observable properties. (b) We consider a three-dimensional band structure,[5] with hopping in the z direction substantially smaller than in the xy plane, as appropriate to the layered oxide materials. (c) We include the effective-mass enhancement correction, which becomes increasingly important as the number of holes in the occupied band decreases. In addition, we have computed various properties of the superconducting state that were not discussed in Ref. 4: London penetration depth, thermodynamic critical field, Knight shift, and Ginzburg-Landau parameters.

Because of the strong universal features of BCS theory, many of the properties of the model discussed here show little difference from what would be obtained from other pairing mechanisms. Characteristic behavior, however, arises when one considers the variation of these properties with hole concentration. While some properties of the high-T_c oxides have already been experimentally studied as a function of doping, most notably the transition temperature,[6-9] many others have not. We hope that in the future these difficult systematic studies will be pursued vigorously, as they offer a promising way to differentiate between proposed alternative mechanisms. In this respect the original 2-1-4 structures appear to offer the most controlled environment as they do not present complications such as charge transfer between chains and planes that can occur in the 1-2-3 structures.

We wish to emphasize here that a complete description of the properties of these materials would require inclusion of the Cu $d_{x^2-y^2}$ orbitals into the problem. For example, these orbitals certainly play an important role in the insulating phase, and give rise to the observed antiferromagnetism. A strong school of thought[10] has taken the point of view that magnetic excitations associated with the Cu orbitals persist into and indeed *cause* the superconducting state to appear. There is, however, anoth-

er growing point of view, which can be called conventional, that maintains the usual idea that magnetism and superconductivity are at best unrelated and at worst antagonistic to one another. The existence of "nonmagnetic" 30 K oxide superconductors, along with the growing consensus that a Fermi-liquid description is appropriate for all the doped materials, is strong supporting evidence for the conventional viewpoint. In this work we have therefore focused on the minimal model that we feel captures the essence of superconductivity in these materials. It is expected that the qualitative results and trends in this work will survive a more detailed model involving Cu $d_{x^2-y^2}$ orbitals. A detailed comparison with experiments will eventually decide between the various competing models and points of view.

This paper is organized as follows: In Sec. II we review the model and formalism, including the new ingredients discussed above, and discuss the choice of parameter values, specifically for the Y-Ba-Cu-O material, based on available experimental information. In Sec. III we investigate the expected dependence of T_c on pressure within this model. T_c is found to increase with pressure applied in the plane, but can decrease with pressure applied uniaxially perpendicular to the planes for a range of hole concentration. In Sec. IV we present results for various superconducting properties. The specific-heat jump and the gap ratio, $2\Delta_0/k_B T_c$, show systematic variation with doping, and become larger than the weak-coupling BCS result at low hole density. Also shown is the London penetration depth and Ginzburg-Landau coherence length in the different directions. Their temperature dependence is close to the universal weak-coupling behavior but they also exhibit systematic trends with doping. Results for the tunneling characteristic are shown, including self-energy and band-structure effects, and the effects of nearest-neighbor repulsion, V. The latter in particular reduces the expected asymmetry described previously,[4] but for realistic parameters the asymmetry is still unambiguously observable (and of universal sign). The expected behavior of Knight shift and NMR relaxation rate within our model is also briefly discussed. In Sec. V we present calculations of the superconducting pair wave function and of the coherence length, ξ_0, defined from the spatial extent of the wave function. At low temperatures it is expected that this coherence length be quite similar to the Ginzburg-Landau coherence length, and we compare the results obtained from both methods. The nature of the pairing interaction together with the effective-mass enhancement effect determine a characteristic behavior of the pair wave function versus doping: For low hole doping the system is in the strong-coupling regime and paired holes are confined to be a single lattice spacing apart, and as the hole doping increases the system gradually crosses over to the weak-coupling regime with the coherence length rapidly increasing. For an isotropic system this crossover was discussed recently.[11] Finally, a summary and discussion of the results are found in Sec. VI. Appendices A and B discuss the derivation of various results used in the paper.

II. QUASI-TWO-DIMENSIONAL MODEL

We consider the single-band Hamiltonian[3,4]

$$H = -\sum_{\substack{ij \\ \sigma}} t_{ij}(c_{i\sigma}^{\dagger}c_{j\sigma}+\text{H.c.}) + U\sum_i n_{i\uparrow}n_{i\downarrow}$$
$$+ \sum_{ij} V_{ij}n_i n_j - \mu\sum_{i\sigma} n_{i\sigma}$$
$$- \sum_{\substack{ij \\ \sigma}} (\Delta t)_{ij}(c_{i\sigma}^{\dagger}c_{j\sigma}+\text{H.c.})(n_{i,-\sigma}+n_{j,-\sigma}) , \quad (1a)$$

where i,j are sites on a three dimensional lattice, $c_{i\sigma}^{\dagger}$ is the creation operator for a hole of spin σ at site i, $n_i \equiv n_{i\uparrow}+n_{i\downarrow}$ is the number operator, U is the Hubbard on-site repulsion, V_{ij} is the Coulomb repulsion between two holes on sites i and j, and μ is the chemical potential. The last term describes the enhanced hopping rate for holes, and we assume

$$(\Delta t)_{ij} = \alpha t_{ij} , \quad (1b)$$

with $\alpha > 0$. In our tight-binding model we take

$$t_{ij} = \begin{cases} t_{\parallel}^h, & i,j \text{ nearest neighbors in the plane} \\ -t_{\perp}^h, & i,j \text{ nearest neighbors out of plane} \\ 0, & \text{otherwise} . \end{cases}$$
$$(2a)$$

Similarly, for the larger range repulsion, we use

$$V_{ij} = \begin{cases} V_{\parallel}, & i,j \text{ nearest neighbors in the plane} \\ V_{\perp}, & i,j \text{ nearest neighbors out of plane} \\ 0, & \text{otherwise} . \end{cases} \quad (2b)$$

and we define

$$\rho = t_{\perp}^h/t_{\parallel}^h , \quad (3a)$$
$$v = V_{\perp}/V_{\parallel} . \quad (3b)$$

The superscript h refers to the fact that these are the values of hopping matrix elements at the bottom of the hole band.

In the copper-oxygen planes of the high-T_c oxide superconductors, the Hamiltonian Eq. (1) describes conduction by direct hopping of oxygen holes between nearest-neighbor oxygens, presumably in $p\pi$ orbitals. The last term in the Hamiltonian Eq. (1a) is strongly attractive for a few holes in such a band. Electrons or holes in oxygen $p\sigma$ orbitals and Cu orbitals are not considered, as we assume they are not essential to superconductivity. We also do not specify precisely which orbitals are involved in conduction perpendicular to the planes, as this is not essential. The assumption [Eq. (1b)] that the hopping interaction and the hopping are proportional with the same proportionality constant in all directions is reasonable in view of the fact that both terms are determined by *the same* overlap matrix element of whichever electronic orbitals are involved.[3] On the other hand, there is no reason for ρ and v in Eq. (3) to be similar, and in particu-

lar v should be much larger than ρ in a layered material as it does not involve wave function overlap factors.

Figure 1 illustrates cross sections of the noninteracting hole Fermi surface expected from such a model, for various hole concentrations. At low hole doping the Fermi surface consists of two pockets enclosing the points $(0,0,\pm\pi)$. Except where important, we suppress reference to the lattice spacing. At higher doping, the pockets meet at $k_z=0$ and eventually form the typical "hourglass" figure. The single-particle energies that follow from Eq. (2) are

$$\varepsilon_k^h = -2t_\parallel^h(\cos k_x a_\parallel + \cos k_y a_\parallel) + 2t_\perp^h \cos k_z a_\perp , \quad (4)$$

where $a_\parallel$ is the in-plane lattice spacing and $a_\perp$ is the spacing in the direction perpendicular to the plane. For small hole filling (4) gives holelike effective masses near the zone boundary ($k_z = \pm\pi$), whereas near the zone center the masses are holelike in the (k_x, k_y) plane but electronlike in the k_z direction. Figure 2 illustrates the effect of hopping in the third direction on the density of states. As is well known, the van Hove singularity at the origin is removed, and the band is broadened beyond that in the two-dimensional case. Discontinuities remain in the first derivative, however, which occur at $\varepsilon_k^h = \pm(4t_\parallel^h + 2t_\perp^h)$, $\pm(4t_\parallel^h - 2t_\perp^h)$, and $\pm 2t_\perp^h$.

For low fillings the Hamiltonian (1) has one important self-energy effect, arising from the enhanced hopping term.[3] The first-order diagram gives a band-broadening contribution, effectively renormalizing t_{ij} to $t_{ij}(1+\alpha n)$. Physically this says that holes have higher effective mass than electrons, since they alter the background wave function in a solid more than electrons do. As holes are added to a filled band, their effective mass becomes increasingly smaller with increasing number of holes.
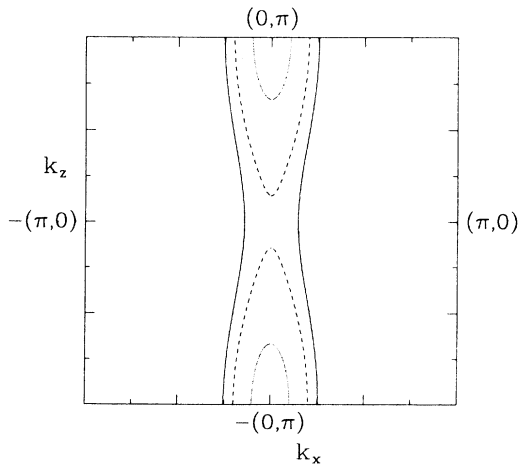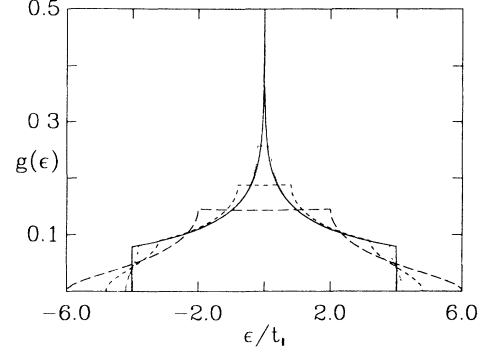
FIG. 2. Single-particle densities of states with nearest-neighbor hopping only. The curves plotted are for $t_\perp = 0$ (solid), $t_\perp = 0.1t_\parallel$ (dotted), $t_\perp = 0.4t_\parallel$ (short dashed) and $t_\perp = 1.0t_\parallel$ (long dashed).

The interaction between Cooper pairs resulting from the Hamiltonian Eq. (1) is

$$V_{kk'} = U + \sum_\delta V_\delta e^{i(k-k')\cdot\delta} - 2\alpha \sum_\delta t_\delta^h(e^{ik\cdot\delta} + e^{ik'\cdot\delta}) , \quad (5)$$

where, as given by Eq. (4), $\varepsilon_k^h = -\sum_\delta t_\delta^h e^{ik\cdot\delta}$. The BCS equation is repeated from Ref. 4, for convenience:

$$\Delta_k = -\frac{1}{N}\sum_{k'} V_{kk'}\Delta_{k'}\frac{1-2f(E_{k'})}{2E_{k'}} , \quad (6a)$$

$$E_k = [(\varepsilon_k - \mu)^2 + \Delta_k^2]^{1/2} \quad (6b)$$

with

$$\varepsilon_k = \varepsilon_k^h(1+\alpha n) \quad (6c)$$

along with the constraint condition for the density of holes, n:

$$n = 1 - \frac{1}{N}\sum_k \frac{\varepsilon_k - \mu}{E_k}[1 - 2f(E_k)] . \quad (6d)$$

In the absence of nearest-neighbor repulsion the form of the gap is not modified by band anisotropy, as discussed in Ref. 5. Here, however, the anisotropic band structure together with the nearest-neighbor Coulomb interaction require an ansatz for the gap:

$$\Delta_k = \Delta_m\left[c - \frac{\varepsilon_k}{4t_\parallel} - c'\cos k_z\right] \equiv \Delta(\varepsilon_k, k_z) , \quad (7)$$

which differs from the form used in Ref. 4 due to the parameter c'. The solution of these equations is discussed in Appendix A. Appendix B discusses the strong-coupling limit of the model, with $t_\parallel = t_\perp = 0$.

If c' in Eq. (7) is zero the gap is constant over the Fermi surface, since $\varepsilon_k = \varepsilon_F$ on it. As shown in Appendix A, with $\rho \equiv t_\perp/t_\parallel = 0$, $c' \equiv 0$ for any value of $v \equiv V_\perp/V_\parallel$. In the opposite extreme, the isotropic three-dimensional case ($\rho = \pm 1, v = 1$), $c' \equiv 0$ also, and furthermore, for $V_\parallel = V_\perp = 0$, $c' \equiv 0$ for all values of ρ. Finally, in the strong-coupling limit, $c' = 0$ for $v = 1$, as shown in Ap-

FIG. 1. Slices $k_y = 0$) of the Fermi surface for three different values of the Fermi energy, $\mu = -4t_\parallel - t_\perp$ (dotted), $\mu = -4t_\parallel + 1.8t_\perp$ (dashed), and $\mu = -4t_\parallel + 4t_\perp$ (solid), for $\rho = 0.1$. The band fillings for these cases are $n = 0.002$, 0.015, and 0.033, respectively. For the parameters shown, the surfaces have almost cylindrical symmetry about the z axis.

pendix B. This suggests that the gap in our model will not be very far from isotropic for any parameters, and in particular that in the physically interesting regime for the high-T_c oxides, small ρ and not too large Vs the effects of anisotropy due to $c' \neq 0$ will be very small. This will be illustrated in the following.

We next discuss the range of parameters in our model expected for the high-T_c oxides in light of the experimental information available. Various measurements have pointed towards appreciable anisotropy in the direction perpendicular to the planes. Resistivity measurements[12] exhibit anisotropies of the order of 40 to 1 for YBa$_2$Cu$_3$O$_{7-\delta}$, although they are quite sensitive to sample quality. Upper critical-field measurements on the same material yield ratios $H_{c2}^{\perp}/H_{c2}^{\parallel}$ ranging from 5–10,[12–14] which translates into the same ratio for the inverse coherence lengths and gives a ratio for the effective masses, which is 25–100. Measurements of the magnetic penetration depth[15] in single crystal YBa$_2$Cu$_3$O$_{7-\delta}$ suggest a ratio of effective masses $m_{\perp}^*/m_{\parallel}^* \gtrsim 25$. These estimates all point towards the fact that the oxides are highly two dimensional. For our purposes the ratio of hoppings needed in the theory is related to the effective masses through the lattice constants:

$$\frac{t_{\perp}}{t_{\parallel}} = \frac{m_{\parallel} a_{\parallel}^2}{m_{\perp} a_{\perp}^2} . \tag{8}$$

Although it is not entirely obvious what the "effective" spacing in the direction perpendicular to the layers is, these experimental results suggest that within our simplified model the ratio of hoppings in both directions should certainly be taken somewhere in the range $t_{\perp}/t_{\parallel} \sim 0.01$–$0.1$, and, fortunately, the properties of the model are not extremely sensitive to this ratio, as will be shown in the following. Hence, we will choose $t_{\perp}/t_{\parallel} = 0.025$ and 0.1 as representative cases (the latter is clearly an upper bound) in most of what follows. On the other hand, the nearest-neighbor Coulomb repulsion is expected to depend less strongly on the interatomic distances, and in addition screening will be larger for holes in the plane. These considerations suggest that choosing $V_{\perp} = V_{\parallel}$, i.e., $v = 1$, is a reasonable estimate.

Next we discuss the choice of in-plane hopping $t_{\parallel}$. Recall that the Hamiltonian Eq. (1) describes holes, and the hopping for holes at the top of the band is related to the hopping of electrons at the bottom of the band, $t_{\parallel}$, by

$$t_{\parallel}^h = t_{\parallel}^e - 2\Delta t_{\parallel} \tag{9}$$

with $\Delta t_{\parallel} = \alpha t_{\parallel}^h$. Equation (9) suggests that $t_{\parallel}^h$ could be very small. More generally, for n holes in the filled band the hopping is renormalized due to the last term in Eq. (1) to

$$t_{\parallel}(n) = t_{\parallel}^e - 2\Delta t + n\Delta t_{\parallel} , \tag{10}$$

and it becomes larger as holes are added to the filled band. The resistivity in the oxides is found to decrease rapidly as holes are added,[7,8] which we interpret to be due to the effective-mass change caused by Eq. (10). For very low density of holes the resistivity turns upward at

low temperatures indicating semiconducting behavior. This suggests that the hopping at the top of the band $t_{\parallel}^h$ is close to zero. We will show results for three cases in what follows: $t_{\parallel}^h = 0.001$, 0.03, and 0.06 eV. It is not impossible that a negative value of $t_{\parallel}^h$ would be applicable, as considered in Ref. 11. However, the results do not change qualitatively even in that case. In the following we discuss additional justification for our choice.

Next we need to specify the values of the interatomic parameters. We define

$$W = zV , \tag{11a}$$

$$K = 2z\Delta t , \tag{11b}$$

with $z = 4$ the number of nearest neighbors in the plane. The constraint that the Coulomb interaction between electrons in antibonding states in the plane be positive translates into the condition[4,11]

$$K < \frac{U + W}{2} , \tag{12}$$

but there is nothing that precludes K from being arbitrarily close to this limit. Hence we will choose, for simplicity,

$$K = \frac{U + W}{2} , \tag{13}$$

assuming we are very close to this "optimal" situation. Choosing somewhat smaller K would only change our results slightly. For given U, Eq. (13) and the maximum T_c desired determine then the values of K and W. It should be noted that an additional constraint on the interactions is $K < 2W$ ($\Delta t < V$) (Ref. 11) which, as we will see, will not conflict with the values obtained from the other conditions.

Figures 3–5 show the critical temperature versus hole concentration for values of $U = 5$, 6.5, and 8 eV, and the three values of $t_{\parallel}^h$, with maximum $T_c = 100$ K in all cases. As explained, the values of K and W are determined by
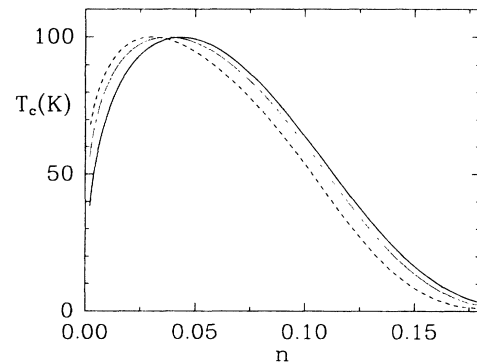

FIG. 3. T_c vs hole concentration for $U = 5.0$ eV, for three values of the hopping amplitude, $t_{\parallel}^h = 0.060$ eV (solid), $t_{\parallel}^h = 0.030$ eV (dotted), and $t_{\parallel}^h = 0.001$ eV (dashed). We have used $\rho = 0.1$ and $v = 1$. The parameters are chosen such that $K = (U + W)/2$. Actual values used are given in Table I.
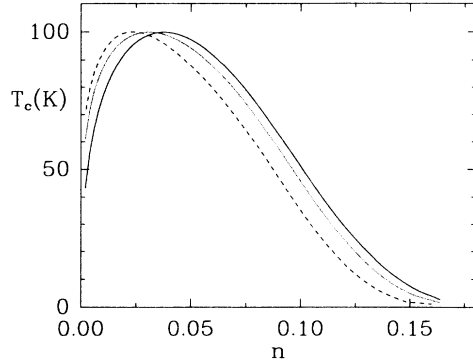
FIG. 4. T_c vs hole concentration for $U = 6.5$. See Fig. 3 for legend and Table I for parameter values.
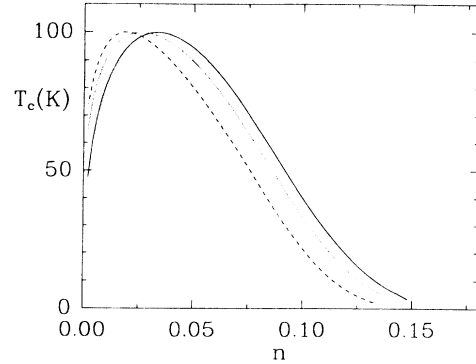

FIG. 5. T_c vs hole concentration for $U = 8.0$. See Fig. 3 for legend and Table I for parameter values.

Eq. (13) and the maximum T_c. We have chosen a hopping anisotropy $\rho = 0.1$. Table I gives the values of the parameters used in all cases. It can be seen that the range of hole concentration where T_c is not zero is somewhat less than 0.2 in all cases [note that $(2n)$ gives the number of holes per CuO_2 unit in the plane]. This range is completely determined by the nature of the model and the constraints on the parameters. In our previous work[4] the range of nonzero T_c was found to be higher because the hopping renormalization Eq. (10) was neglected. Here, the fact that the effective mass becomes smaller as holes are added, together with the fact that the hopping interaction becomes less attractive as holes are added, cause T_c to go to zero beyond this narrow range. For larger U, a larger Δt is required for a maximum $T_c = 100$ K. This causes T_c to go to zero at a somewhat lower hole concentration, since the effective hopping parameter given by Eq. (10) increases more quickly.

Within our tight-binding model the hopping is related to the effective mass by

$$t_\parallel = \frac{\hbar^2}{2m_\parallel^* a^2} , \tag{14}$$

which yields, for the high-T_c oxides with planar oxygen distances $a \sim 2.7$ Å the relation

$$t_\parallel = 0.52 \frac{m_e}{m_\parallel^*} \tag{15}$$

with m_e the free electron mass and $t_\parallel$ in eV. Several experiments have indicated a substantial mass enhancement in the oxides. In particular, measurements of the penetration depth[15] and optical experiments[16] have suggested $m^*/m_e \sim 8-10$ in the 90 K materials. This yields, through Eq. (15), an in-plane hopping amplitude $t_\parallel \sim 0.05-0.065$ eV, and an in-plane bandwidth of $8t_\parallel \sim 0.4-0.5$ eV. This is consistent with recent angle resolved photoemission experiments[17] that indicate the existence of a narrow-band crossing the Fermi level of width approximately 0.5 eV. In our model the effective hopping depends on the hole concentration through Eq. (10); unfortunately, there are no systematic studies of effective mass or effective bandwidth versus doping yet. In Table I we list the values of the effective bandwidth in the plane

TABLE I. Parameters used for the T_c versus density curves in Figs. 3–5. The parameters V and Δt were chosen to satisfy Eq. (13) and yield a maximum T_c of 100 K. $\rho = 0.1$, $v = 1$. $D_\parallel$ denotes the effective bandwidth Eq. (16).

$t_\parallel^h$ (eV)	Δt (eV)	V (eV)	$D_\parallel$ ($n = 0.04$) eV	$D_\parallel$ ($n = 0.08$) eV
		$U = 5$ eV		
0.001	0.463	0.603	0.156	0.304
0.03	0.429	0.467	0.377	0.514
0.06	0.399	0.346	0.608	0.735
		$U = 6.5$ eV		
0.001	0.624	0.870	0.208	0.407
0.03	0.585	0.716	0.427	0.614
0.06	0.553	0.585	0.657	0.834
		$U = 8$ eV		
0.001	0.787	1.148	0.260	0.512
0.03	0.745	0.978	0.478	0.717
0.06	0.709	0.836	0.706	0.934

$$D_\parallel(n) = 8t_\parallel(n) \qquad (16)$$

for two values of n where T_c is close to the maximum, $n = 0.04$ and 0.08. [The total bandwidth is $D_\parallel(n)(1 + \rho/2)$.] The effective-mass enhancement, from Eq. (15), is

$$\frac{m_\parallel^*(n)}{m_e} = \frac{4.16 \text{ eV}}{D_\parallel(n)} . \qquad (17)$$

It can be seen that our largest $t_\parallel^h$ (0.06 eV) yields band widths that are generally somewhat too large to be consistent with the experiments already mentioned, while $t_\parallel^h = 0.03$ eV yields more consistent values. On the basis of this data we will present some results mostly for the values $t_\parallel^h = 0.03$ eV and $U = 5$ eV. As seen from the results in Table I, a negative value of $t_\parallel^h$ would yield too narrow a band to be consistent with these experiments, although it may be justifiable in a model where other bands are included.

We now examine the effect of varying the hopping in the third direction. Figure 6 shows T_c versus n for $\rho = 0$, 0.1, and 0.2. It can be seen that the results are very insensitive to the degree of anisotropy. This remains true for larger anisotropies, as shown in Fig. 7. In Figs. 8 and 9 we show the effect of hopping in the third direction on the gap anisotropy, defined by

$$\eta = \frac{\Delta(\mu,\pi) - \Delta(\mu,0)}{\Delta(\mu,\pi) + \Delta(\mu,0)} = \frac{c'}{c - \mu/4t_\parallel} , \qquad (18)$$

which measures the relative variation of the gap on the Fermi surface. It can be seen that the anisotropy remains remarkably small for all cases, for the reasons discussed in the paragraph after Eq. (7). Our model leads to the somewhat paradoxical result that as we move from a highly anisotropic structure towards a more isotropic one the superconducting state first becomes increasingly anisotropic before it again becomes isotropic as $\rho \to 1$.

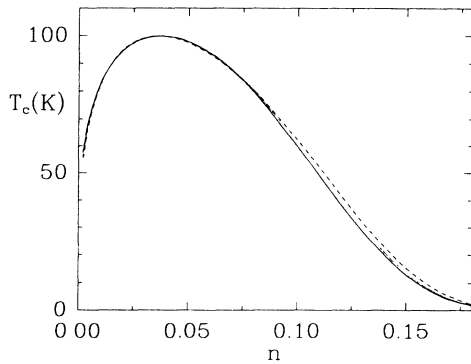FIG. 7. T_c vs hole concentration for $U = 5$ eV, $t_\parallel^h = 0.03$ eV, $v = 1$, for various values of hopping anisotropy: $\rho = 0$ (solid), $\rho = 0.2$ (dotted), $\rho = 0.4$ (short dashed), and $\rho = 1.0$ (long dashed). The value of Δt was fixed at 0.463 eV, and $V_\parallel$ was adjusted so that the maximum $T_c \approx 100$ K.

It is worth emphasizing the remarkable simplicity of the hole mechanism of superconductivity with regard to anisotropy. Because the superconductivity is driven by an attraction originating in a hopping process, the same type of process that gives rise to the band energy, the superconducting state is *intrinsically* isotropic, regardless of the band structure. This does not preclude coherence lengths and penetration depths from being very anisotropic, but it forces the superconducting gap to be isotropic, i.e., constant over the Fermi surface. As already seen, some anisotropy in the gap can arise because of repulsive interactions such as the nearest-neighbor repulsion considered here, which will not have the same anisotropy as the hopping, but the nature of the model restricts the anisotropy to be small. For the regime appropriate to the high-T_c oxides the gap, as shown above (Fig. 8), is very nearly isotropic, and so we will proceed for the most part with a model where the interactions are isotropic, given by

FIG. 6. T_c vs hole concentration for $U = 5$ eV and $t_\parallel^h = 0.03$ eV, for three values of the interplanar hopping, $t_\perp = 0$ (solid), $t_\perp = 0.1t_\parallel$ (dotted), and $t_\perp = 0.2t_\parallel$ (dashed). T_c vs n is clearly insensitive to small values of interplanar hopping. Δt and V were chosen to satisfy $K = (U + W)/2$ such that the maximum $T_c \approx 100$ K. $v = 1$ was used.
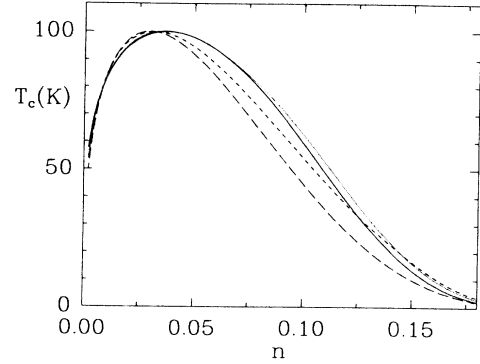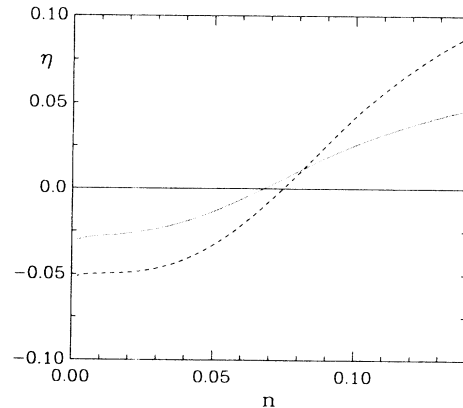

FIG. 8. Gap anisotropy η (Eq. 18) vs hole concentration, for $\rho = 0.1$ (dotted) and $\rho = 0.2$ (dashed). The curves shown reflect the gap anisotropy at T_c. There is very little change at $T = 0$. Curves are for the parameters of Fig. 6.
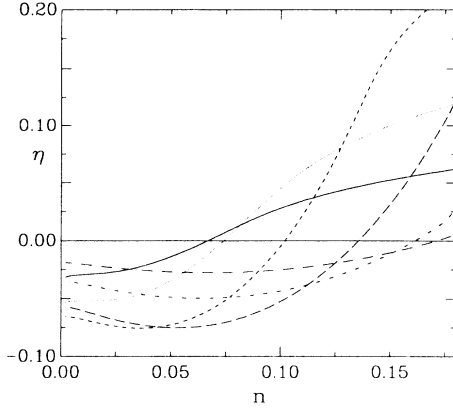
FIG. 9. Gap anisotropy vs hole concentration for larger values of the hopping anisotropy. The curves plotted are for $\rho=0.1$ (solid), $\rho=0.2$ (dotted), $\rho=0.4$ (short dashed), $\rho=0.6$ (long dashed), $\rho=0.8$ (dotted short dashed), and $\rho=0.9$ (dotted long dashed). For $\rho=0$ or $\rho=1$, there is no gap anisotropy. Note that the magnitude of the gap anisotropy is greatest for intermediate values of hopping anisotropy, though still less than 10% for most of the range of concentrations. Curves were obtained with $U=5$ eV, $t_\parallel^h=0.03$ eV, and $v=1$. See Table I.

$$V_{kk'}=U+W\left[\frac{\varepsilon_k}{4t_\parallel}\right]\left[\frac{\varepsilon_{k'}}{4t_\parallel}\right]+K\left[\frac{\varepsilon_k}{4t_\parallel}+\frac{\varepsilon_{k'}}{4t_\parallel}\right],\qquad(19)$$

where $W\equiv4V_\parallel$ and $K\equiv8\alpha t_\parallel$. Within this model the only momentum dependence in the interaction is in directions orthogonal to the constant energy surfaces, and in particular orthogonal to the Fermi surface. We have, however, retained hopping anisotropy, which is implicit in the ε_k's in Eq. (19), for example. Curves of T_c versus n for this model are indistinguishable from the ones shown in Fig. 6. Before adopting this simplified model, however, it is necessary to keep the full momentum dependence of the interaction, Eq. (5) to calculate the pressure dependence of T_c within our model, which is the subject of Sec. III.

III. PRESSURE DEPENDENCE OF T_c

As is well known, the early finding of a large positive pressure derivative in the oxides was one of the most striking features of the new materials, and led to the discovery of superconductivity above liquid nitrogen temperatures.[18] Within our model a large positive pressure derivative arises naturally because the attractive hopping interaction is enhanced when the lattice spacing decreases. However, the behavior is different for pressure applied in the plane and perpendicular to the planes and has a characteristic density dependence which we will discuss in detail here.

Some recent experimental reports on changes in T_c versus pressure exist, for both uniaxial and isotropic pressure,[19] and also for the density dependence of the pressure derivative.[7] Our predictions do not agree in detail with these results, and possible reasons for the discrepan-

cy will be discussed during the course of this section.

We assume that the only effect of pressure is to change the hopping matrix elements $t_\parallel$ and $t_\perp$, as well as the hopping interaction parameters $\Delta t_\parallel$ and $\Delta t_\perp$ (leaving the ratio α fixed). This is a reasonable assumption, as the dominant effect of pressure will be to change the distance between lattice sites and hence the overlap of the wave functions. If a is the lattice spacing between oxygens in the plane we have approximately

$$t_\parallel=\alpha e^{-\beta a}.\qquad(20)$$

A differential increase in pressure dP in the plane induces a corresponding change in a:

$$dP=-\frac{da}{\gamma_\parallel},\qquad(21)$$

and the change in hopping is

$$\frac{dt_\parallel}{t_\parallel}=\beta\gamma_\parallel dP.\qquad(22)$$

We will calculate the fractional change in T_c under a fractional change of the hopping:

$$\frac{d\ln T_c}{d\ln t_\parallel}=\frac{1}{\beta\gamma_\parallel}\frac{d\ln T_c}{dP},\qquad(23)$$

and an analogous relation exists with pressure applied perpendicular to the planes. The parameters $\gamma_\parallel$ and $\gamma_\perp$ could easily be measured experimentally, but to our knowledge this has not yet been done in systematic studies of T_c versus pressure. They are surely a small fraction of Å per kbar, with $\gamma_\parallel$ probably smaller than $\gamma_\perp$. The parameter β could be estimated accurately from quantum-chemical calculations, and should be of order one inverse Å.

Figures 10 and 11 show $d\ln T_c/d\ln t_\parallel$ for various values of the parameters. In all cases the pressure derivative is large and positive, and increases rapidly with hole concentration. A smaller in-plane hopping increases the pressure derivative, and so does an increasing on-site repulsion U. The parameters were chosen according to the prescription discussed in Sec. II so that the maximum T_c is 100 K.

Figures 12 and 13 show the same cases for pressure applied perpendicular to the planes. Note the different ordinate scales in these figures compared to Figs. 10 and 11. The trends are the same as for in-plane pressure, but the size of the effect is significantly smaller. In addition, the pressure derivative here can become negative for small values of n and not too small hopping.

We can understand these features in various limiting cases. Consider the expressions for the transition temperature for an isotropic model. In weak coupling we have (assuming a constant density of states)

$$k_B T_c=\frac{e^\gamma}{\pi}D\sqrt{n(2-n)}e^{-a/b},\qquad(24a)$$

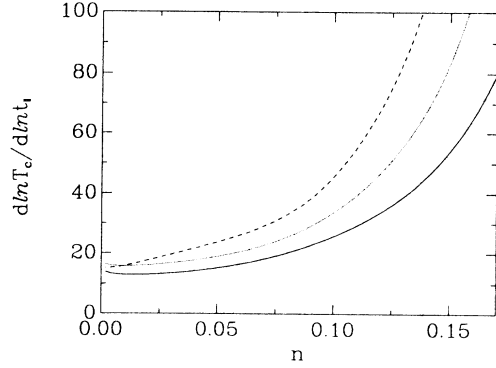$$a=1+2k(1-n)-w(1-3n+\tfrac{3}{2}n^2)+(k^2-wu)(1-n)^2,\qquad(24b)$$

FIG. 10. Plot of the dimensionless pressure derivative, $d\ln T_c/d\ln t_\parallel$, for pressure applied in the plane, for $t_\parallel^h = 0.06$ eV (solid), $t_\parallel^h = 0.03$ eV (dotted), and $t_\parallel^h = 0.001$ eV (dashed). We have used $U = 5$ eV, with $\rho = 0$ and Δt and V chosen such that $K = (U + W)/2$ and the maximum $T_c = 100$ K, as before. We find a substantial increase of the pressure derivative as a function of doping. For the case $t_\parallel^h = 0.001$ eV, we have used $\Delta t = 0.46$ eV and $V_\parallel = 0.59$ eV. Note that the limiting value of the pressure derivative as $n \rightarrow 0$ agrees very well with that obtained from the strong-coupling limit, from Eqs. (27) ($d\ln T_c/d\ln t_\parallel = 15.3$).

FIG. 12. Plot of dimensionless pressure derivative, $d\ln T_c/d\ln t_\perp$, for pressure applied in the direction normal to the planes. We have used $U = 5$ eV, $\rho = 0.1$, $v = 1$, and $t_\parallel^h = 0.06$ eV (solid), 0.03 eV (dotted), and 0.001 (dashed). See Table I for parameters values. For the lowest value of the hopping parameter (dashed curve), the curve remains positive and the strong-coupling limit, Eq. (30), is achieved as $n \rightarrow 0$. For higher values of the interplanar hopping, the derivative is actually negative at low hole concentrations. Note that the overall magnitude of the pressure derivative is significantly smaller than for pressure applied in the planes (Figs. 10 and 11).

$$b = 2k(1-n) - w(1-n)^2 - u + (k^2 - wu)\left[1 - n + \frac{n^2}{2}\right],$$
(24c)

with $k = K/D$, $u = U/D$, $w = W/D$, and the bandwidth D given by

$$D = 2z(t^h + n\Delta t)$$
(25a)

and

$$K = 2z\Delta t,$$
(25b)

$$W = zV,$$
(25c)

with z the number of nearest neighbors. For a change in t we have

$$\frac{dk}{d\ln t} = 0,$$

$$\frac{du}{d\ln t} = -u,$$

$$\frac{dw}{d\ln t} = -w.$$

Thus, the normalized on-site and nearest-neighbor repulsion decrease while the hopping interaction does not, leading to an increase in T_c driven by the change in the exponent (the prefactor gives a contribution of the same sign). The result is
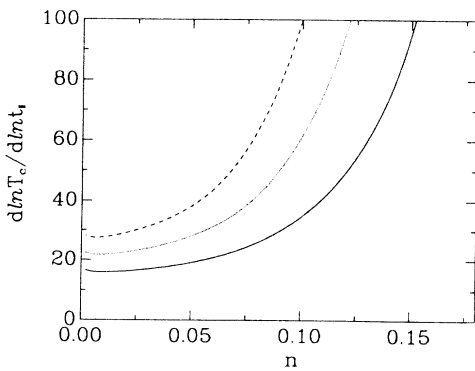

FIG. 11. Same as Fig. 10 except $t_\parallel^h = 0.03$ eV and $U = 5$ eV (solid), 6.5 eV (dotted), and 8 eV (dashed). In all cases the pressure derivative is positive and increases with doping.
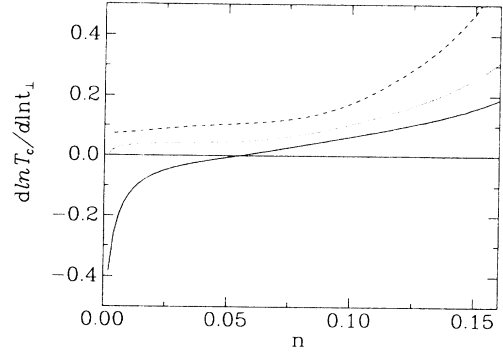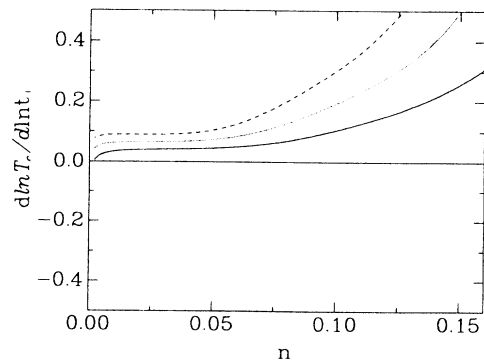

FIG. 13. Same as Fig. 12 except $t_\parallel^h = 0.03$ eV and $U = 5$ (solid), 6.5 eV (dotted), and 8 eV (dashed).

$$\frac{d\ln T_c}{d\ln t} = 1 + \frac{\phi}{b^2} , \qquad (26a)$$

$$\phi = u(1+kx)^2 + wx^2(1+u)^2 + w(1-x^2)$$

$$\times \left[u + kx(1+2u) + \frac{k^2+uw}{u}(1-x^2) \right] , \qquad (26b)$$

$$x = 1 - n , \qquad (26c)$$

and it can be seen that it is always positive, and that increasing u, w, and k make the pressure derivative larger, as does an increase in n.

In strong coupling the critical temperature is given for constant density of states by[11]

$$k_B T_c = \frac{1-n}{2\ln(2/n-1)} E_b , \qquad (27a)$$

$$E_b = \left[\frac{1}{4}\left[U + \frac{W}{3} \right]^2 + \frac{K^2 - WU}{3} \right]^{1/2} - \frac{1}{2}\left[U + \frac{W}{3} \right] , \qquad (27b)$$

so that

$$\frac{d\ln T_c}{d\ln t} = \frac{K^2}{3E_b}\frac{1}{E_b + \frac{1}{2}(U+W/3)} , \qquad (27c)$$

which also increases as K increases and E_b decreases [as occurs if U is increased and the parameters satisfy Eq. (13)].

Comparison of these analytic results with results from the numerical solution of the BCS equations is shown in Fig. 14. At high densities the system is in the weak-coupling regime and the results agree with those given by Eq. (26). As the density is lowered the system approaches the strong-coupling regime, and the pressure derivative becomes larger than the weak-coupling result. For the case shown in Fig. 14(b), $t_\parallel^h = 0.001$, the strong-coupling limit is achieved as $n \to 0$ and the pressure derivative approaches the result Eq. (27c).

The different magnitude of the pressure derivative in the direction parallel and perpendicular to the planes is most easily seen in the strong-coupling limit. For our lattice model Eq. (27a) still holds, while the binding energy, as shown in Appendix B, is given by

$$E_b = \left[\frac{(U+W/4)^2}{4} + \frac{K^2(1+\rho^2/2)-WU}{4} \right]^{1/2}$$

$$- \frac{1}{2}\left[U + \frac{W}{4} \right] \qquad (28)$$

so that we obtain

$$\frac{d\ln k_B T_c}{d\ln t_\parallel} = \frac{K^2}{4E_b\{E_b + [U+(W/4)]/2\}} \qquad (29)$$

and

$$\frac{d\ln k_B T_c}{d\ln t_\perp} = \frac{1}{2}\rho^2 \frac{d\ln k_B T_c}{d\ln t_\parallel} \qquad (30)$$

so that for $\rho = 0.1$ the ratio is $\frac{1}{200}$. This is in agreement

with the limiting results in Figs. 10 and 12 for $U = 5$, $t_\parallel^h = 0.001$, as $n \to 0$. Note that the pressure derivative is positive in the strong-coupling limit. The negative pressure derivative in Fig. 12 corresponds to the largest $t_\parallel^h$, where the strong-coupling limit is not reached as $n \to 0$.

In weak coupling, the different behavior of the pressure derivative in and perpendicular to the planes can also be understood qualitatively. The lower band edge is given by

$$\varepsilon_l = -4t_\parallel - 2t_\perp \qquad (31a)$$

and the position of the first Van Hove singularity by

$$\varepsilon_{VH} = -4t_\parallel + 2t_\perp \qquad (31b)$$

(see Fig. 2). The effect of increasing $t_\parallel$ is to broaden the band, lowering both ε_l and ε_{VH} by the same amount. This causes the Fermi energy to shift to a lower value and give a larger attractive interaction, from Eq. (19). On the other hand, increasing $t_\perp$ shifts ε_l down and ε_{VH} up by the same amount. If ε_F lies to the right of ε_{VH} it is found to be left unchanged to lowest order in $t_\perp/t_\parallel$, leading to no change in the attractive interaction at the Fermi
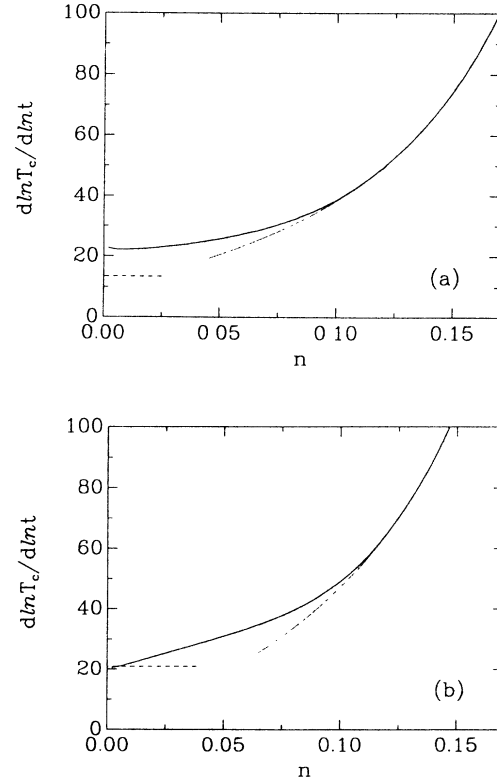

FIG. 14. Pressure derivative for two-dimensional model with constant density of states. The bandwidth is $D = 8(t_h + n\Delta t)$, and $U = 5$ eV. (a) $t^h = 0.03$ eV, $V = 0.56$ eV, $\Delta t = 0.45$ eV; (b) $t^h = 0.001$ eV, $V = 0.66$ eV, $\Delta t = 0.48$ eV. The solid lines give the results for numerical solution of the BCS equations, and the dotted and dashed lines the weak- and strong-coupling limiting forms Eqs. (26) and (27).

surface. A small enhancement of the density of states at ε_F occurs, leading to a small increase in T_c. On the other hand, if ε_F is below $\varepsilon_{\mathrm{VH}}$ two competing effects occur: ε_F is shifted down as $t_\perp$ increases but the density of states at ε_F is reduced substantially. The net effect can be a negative pressure derivative for small hole density, as shown in one of the cases in Fig. 12.

Unfortunately, various effects can occur when pressure is applied to a high-T_c oxide. It is not obvious what the relative change in the various lattice constants is under hydrostatic pressure, nor even under uniaxial pressure. In addition, charge could be transferred between different regions of the structure, leading to a change in the hole concentration in the Cu-O planes under pressure. Thus, a comparison between our calculated changes and existing experiments is not straightforward. We hope that in the future careful hydrostatic and uniaxial pressure experiments as a function of hole concentration will be made, and at the same time the change in lattice constants and the behavior of the Hall coefficient with and without pressure applied will be measured. At this point our results disagree with at least two of the published experimental features: We find no upturn in the pressure derivative at low hole concentration within our model, as found in Ref. 7, and we find a marked difference in the pressure dependence parallel and perpendicular to the planes, in disagreement with the conclusion of Ref. 19 that isotropic pressure and uniaxial pressure in the z direction have approximately the same effect.

IV. OTHER OBSERVABLES

In this section we will discuss several properties in the superconducting state. We wish to explore the detailed temperature dependence of these properties, as well as the behavior as a function of filling. Differences from the universal results of weak-coupling BCS theory will arise for three reasons. First, this mechanism gives rise to an energy dependence of the interaction which is *asymmetrical* with respect to the Fermi surface. Second, the fact that the Fermi level in the normal state lies close to the bottom of the (hole) band here has important consequences. Finally, a related effect is that the model does not necessarily lie in the weak-coupling limit. Indeed, as discussed in Ref. 11, for a given set of parameters, we expect a continuous transition from weak coupling at the maximum hole densities to the intermediate or strong-coupling regime at low hole densities.

A. The penetration depth

The high-T_c oxides are without a doubt in the London limit; i.e., the penetration depth is much larger than the coherence length. For definiteness we will adopt the clean limit. The London kernel is given by[20] $K_{\mu\nu}(q=0)=\delta_{\mu\nu}K_\nu(0)$, where

$$K_\nu(0)=\frac{8\pi e^2}{c^2}\frac{1}{N}\sum_k v_\nu^2\left[\frac{\partial f(E_k)}{\partial E_k}-\frac{\partial f(\varepsilon_k-\mu_n)}{\partial\varepsilon_k}\right] \quad (32)$$

and $v_\nu\equiv(1/\hbar)(\nabla_k\varepsilon_k)_\nu$. (Here $\nu=\perp$, or $\parallel$, with respect to

the Cu-O planes.) An expression such as (32) assumes that screening currents can be described by single-particle hops. While the quasiparticle dressing $\varepsilon_k\equiv\varepsilon_k^0(1+\alpha n)$ extends the validity of Eq. (32) to some extent, it is clear that a breakdown occurs in the strong-coupling limit (see the following), so that our results are not valid in this case. Equation (32) becomes

$$K_\nu(0)=\frac{8\pi e^2}{(\hbar c)^2}\int_{-D/2}^{D/2}d\varepsilon\,g_\nu(\varepsilon)\left[\frac{\partial f(E)}{\partial E}-\frac{\partial f(\varepsilon-\mu_n)}{\partial\varepsilon}\right],$$

$$(33)$$

where

$$\frac{g_\nu(\varepsilon)}{g(\varepsilon)}\equiv\frac{(1/N)\sum_k|\nabla_k\varepsilon_k|_\nu^2\delta(\varepsilon-\varepsilon_k)}{(1/N)\sum_k\delta(\varepsilon-\varepsilon_k)} \quad (34)$$

is the average of the squared velocity in a direction ν ($\equiv x, y$, or z) on a momentum shell of constant energy, ε. $D=8t_\parallel+4t_\perp$ is the bandwidth. The penetration depth is given by

$$\lambda_\nu=\frac{1}{\sqrt{K_\nu(0)}}. \quad (35)$$

The single-particle density of states $g(\varepsilon)$, along with
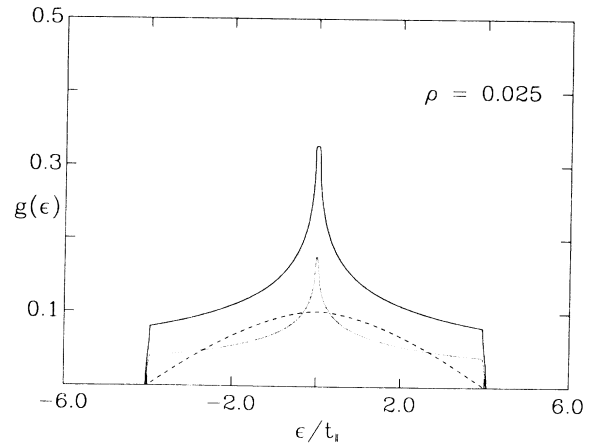

FIG. 15. Single-particle densities of states for nearest-neighbor hopping and $\rho=0.025$. The single-particle density of states is given by the solid curve. The dotted and dashed curves are the Brillouin zone averages associated with the average velocities, $g_\perp(\varepsilon)$ and $g_\parallel(\varepsilon)$, respectively. The actual curves plotted are $1/N\sum_k\sin^2k_z\delta(\varepsilon-\varepsilon_k)\equiv g_\perp(\varepsilon)/4t_\perp^2$ (dotted) and $1/N\sum_k\sin^2k_x\delta(\varepsilon-\varepsilon_k)\equiv g_\parallel(\varepsilon)/4t_\parallel^2$ (dashed). Note that the effective-mass approximation, $g_\perp(\varepsilon)/g_\parallel(\varepsilon)=1/\rho$, is only valid in the very small region at the bottom (and top) of the band where $g_\perp(\varepsilon)$ is rising sharply.

$g_\parallel(\varepsilon)$ [$\equiv g_x(\varepsilon)$ or $g_y(\varepsilon)$] and $g_\perp(\varepsilon)$ are illustrated in Fig. 15, for the case $\rho=0.025$. We will refer to these in the following. In the zero-temperature limit, the penetration depth becomes

$$\lambda_\nu = \frac{\hbar c}{e} \frac{1}{\sqrt{8\pi g_\nu(\mu_n)}} , \tag{36}$$

where μ_n is the chemical potential in the normal state. For an ellipsoidal Fermi surface, this reduces to the standard form:

$$\lambda_\nu = \left[\frac{m_\nu^* c^2}{4\pi n e^2} \right]^{1/2} . \tag{37}$$

This latter result is within the effective-mass approximation. One then obtains the often quoted result, $\lambda_\perp/\lambda_\parallel = (m_\perp^*/m_\parallel^*)^{1/2}$, for example. It is clear, however, from either Fig. 2 or Fig. 15, that expression (37) is only applicable in the extremely low-density limit. The correct expression is Eq. (36), and thus we obtain:

$$\frac{\lambda_\perp}{\lambda_\parallel} = \left[\frac{g_\parallel(\mu_n)}{g_\perp(\mu_n)} \right]^{1/2} = \left[\frac{\langle v_\parallel^2 \rangle_{FS}}{\langle v_\perp^2 \rangle_{FS}} \right]^{1/2} , \tag{38}$$

where $\langle v_\nu^2 \rangle_{FS}$ is the Fermi surface average of the squared velocity in the ν direction. Inspection of Fig. 15 shows clearly that at higher densities the anisotropy ratio can exceed $t_\parallel/t_\perp$, whereas as $n \to 0$,

$$\lambda_\perp/\lambda_\parallel = (t_\parallel s_\parallel^2/t_\perp a_\perp^2)^{1/2} = (m_\parallel^*/m_\perp^*)^{1/2}$$

as in the effective-mass approximation. In order to compute the effective-mass anisotropy for all densities, we adopt the lattice spacings $a_\parallel = 2.7$ Å and $a_\perp = 5.9$ Å. These values are representative of the oxygen-oxygen ion separation in the CuO$_2$ planes in the 1:2:3 compound.[21] In Fig. 16, we plot the ratio $\lambda_\perp/\lambda_\parallel$ at $T=0$ versus hole concentration for $\rho=0.025$, 0.05, and 0.1 along with T_c versus n for the case $\rho=0.025$ (right-hand scale). For $\rho=0.05$ and 0.1, T_c versus n is barely distinguishable from the curve plotted. As we will see in the following, within Ginzburg-Landau (GL) theory,[22] $\lambda_\perp/\lambda_\parallel = H_{c2}^\parallel/H_{c2}^\perp = \xi_{GL}^\parallel/\xi_{GL}^\perp$, where H_{c2} is the upper critical field and ξ_{GL} is the Ginzburg-Landau coherence length. Many estimates of the effective-mass anisotropy have been made from measurements of either of the preceding ratios. At a doping that gives rise to a maximum T_c, the ratio $\lambda_\perp/\lambda_\parallel$ has been estimated[15] to be between 5 and 10. Hence the curve corresponding to $\rho=0.025$ in Fig. 16 appears to be most representative, and shows that as a function of doping a large and measurable change in the "effective-mass" anisotropy [as determined by $\lambda(0)$ or H_{c2}] is expected as a function of filling. The actual values of $\lambda(T=0)$ that we obtain are a factor of 3 or 4 too large. This we attribute to two causes: (1) we have excluded other bands from our description, whose charge carriers will contribute to the Meissner effect but which in our view are unessential to the mechanism that drives super-

conductivity, and (2) Equation (36) overestimates the penetration depth because currents due to pair hopping processes are not included (see Sec. V). The narrow bandwidth we have chosen makes our model extreme type II ($\lambda \gg \xi_{GL}$) for most of the filling range, so that a quantitative comparison with experimental results is not possible. However, we expect the trends as a function of filling to remain, as these are predominantly due to the band driving the superconductivity. In Fig. 17 we plot $\lambda_\parallel(T=0)$ normalized to its value at $n=0.037$ (the filling corresponding to the maximum T_c) versus hole concentration. The divergence as $n \to 0$ occurs slightly faster than expected from the London formula since the effective mass in our model increases as $n \to 0$.

The temperature dependence of the penetration depth is best exhibited by plotting the "deviation" function

$$D_L \left[\frac{T}{T_c} \right] = \frac{\lambda_L^2(0)}{\lambda_L^2(T)} - \left[1 - \left[\frac{T}{T_c} \right]^4 \right] , \tag{39}$$

which emphasizes the deviations from the two-fluid-model result,

$$\lambda_L(T) = \lambda_L(0)/[1-(T/T_c)^4]^{1/2} .$$

In Fig. 18 we have plotted the result for the case $t_\parallel^h = 0.03$ eV, and $U=5$, with $\rho=0.025$. The curves plotted are for $n=0.037$, which gives a maximum $T_c \approx 100$ K. Also included is the weak-coupling BCS result, which exhibits a minimum at $T/T_c = 0.75$ of value -0.21. Note that with field applied normal (parallel) to the plane, the deviation function is smaller (larger) in magnitude at all temperatures. This trend is enhanced even further at lower densities. For example, at $n=0.002$, the minimum value for field applied parallel to the plane is
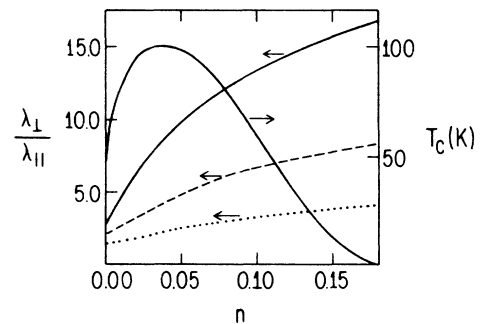

FIG. 16. Plot of the ratio $\lambda_\perp/\lambda_\parallel(=H_{c2}^\parallel/H_{c2}^\perp = \xi_{GL}^\parallel/\xi_{GL}^\perp)$ vs hole concentration for $\rho=0.025$ (solid), $\rho=0.05$ (dotted), and $\rho=0.1$ (dashed). We have used $a_\parallel = 2.7$ Å and $a_\perp = 5.9$ Å, as discussed in the text. The anisotropy ratio is expected to increase as a function of doping, as indicated. Also shown is T_c vs n (right-hand scale) for the case $\rho=0.025$. We have used $U=5$ eV, $\Delta t = 0.428$, $V=0.461$ eV, and $t_\parallel^h = 0.03$ eV. T_c vs n for the other anisotropies is very similar. Similar results for parameters giving a maximum $T_c \approx 40$ K are obtained, though the hole range where T_c is nonzero is smaller (maximum $n \approx 0.11$).

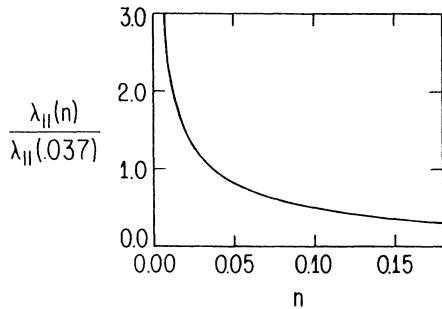FIG. 17. Plot of the normalized penetration depth $\lambda_\parallel(n)/\lambda_\parallel(n=0.037)$ vs hole concentration.

$D_L \approx -0.02$ whereas it is $D_L \approx -0.62$ for field normal to the plane. Conversely, as n increases (and T_c decreases), both curves eventually become indistinguishable from the weak-coupling BCS result. These trends are further enhanced as the bandwidth becomes smaller.

B. Ginzburg-Landau parameters

The fundamental parameter of Ginzburg-Landau (GL) theory is κ, which can be defined in one of two ways:

$$\kappa(T) \equiv \frac{\lambda(T)}{\xi_{GL}(T)} \equiv \frac{1}{\sqrt{2}} \frac{H_{c2}(T)}{H_c(T)} .   (40)$$

Here $\xi_{GL}(T)$ is the GL coherence length, $H_{c2}(T)$ is the upper critical field, and $H_c(T)$ is the thermodynamic critical field. The value of κ determines whether the material is type I or type II, as the second relation explicitly indicates. One also defines within GL theory:

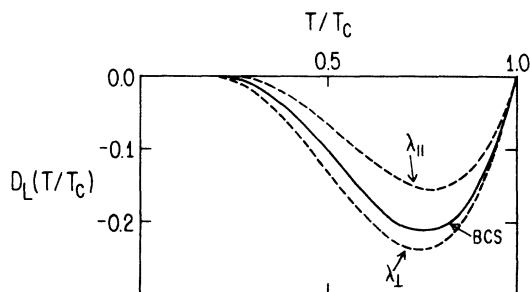$$H_{c2}(T) = \frac{\Phi_0}{2\pi \xi_{GL}^2(T)} ,   (41)$$

FIG. 18. Temperature dependence of the penetration depth for the parameters of Fig. 15, with $\rho = 0.025$, and $n = 0.037$ (maximum $T_c \approx 100$ K). We have plotted the deviation function, $D_L(T/T_c) = \lambda_L^2(0)/\lambda_L^2(T) - [1 - (T/T_c)^4]$, which subtracts off the two-fluid-model result. The deviation for $\lambda_\perp(\lambda_\parallel)$ is larger (smaller) in magnitude than the weak-coupling BCS result. At lower densities, this trend is even more pronounced.

where Φ_0 is the fluxoid quantum ($\Phi_0 = 2.07 \times 10^{-7}$ G cm^2). Using (40) and (41), one can determine $\xi_{GL}(T)$ and hence $H_{c2}(T)$ from microscopic calculations of $\lambda(T)$ and $H_c(T)$. This connection is only exact near T_c. For example, using the London penetration depth to calculate $\lambda(T)$, we obtain

$$H_{c2}(0)/[T_c|H'_{c2}(T_c)|] = 0.66 \text{ and } 0.88$$

in the clean and dirty limits, respectively, whereas the results from microscopic theory are 0.727 and 0.693, respectively.[23] We will proceed nonetheless with GL analysis, since the discrepancy is small as $T \to 0$. For a layered material, we obtain

$$\xi_{GL}^{\perp,\parallel}(T) = \frac{\Phi_0}{2\sqrt{2}\pi H_c(T)\lambda_{\perp,\parallel}(T)}   (42)$$

and

$$H_{c2}^\perp(T) = \frac{\Phi_0}{2\pi \xi_{GL}^{\parallel 2}(T)} ,   (43a)$$

$$H_{c2}^\parallel(T) = \frac{\Phi_0}{2\pi \xi_{GL}^\parallel(T)\xi_{GL}^\perp(T)} .   (43b)$$

The latter two relations are often used to extract coherence lengths at $T = 0$. This is done from measurements of the upper critical field near T_c, through an interpolation formula, such as

$$H_{c2}(0) = 0.69 \ T_c|H'_{c2}(T_c)| .$$

Besides the slight numerical discrepancy already noted, these values are in error because Pauli limiting has not been considered. Nonetheless, we follow the same procedure here. In the next section we will compute and compare the root-mean-square radius of the BCS pair amplitude, $\langle R^2 \rangle^{1/2}$, which should provide a more accurate estimate of the "coherence length."

To calculate the GL coherence length, we need the thermodynamic critical field, $H_c(T)$. It is related to the free energy by

$$H_c(T) = \sqrt{-8\pi\Delta F(T)} ,   (44)$$

where

$$\Delta F(T) \equiv F_s(T) - F_n(T)$$

is the free-energy difference between superconducting and normal states. The free energy is[24]

$$F_s = 2\sum_k n_k \varepsilon_k - \frac{1}{N}\sum_k \frac{\Delta_k^2}{2E_k}[1 - 2f(E_k)]$$

$$+ \frac{2}{N\beta}\sum_k \{[1 - f(E_k)]\ln[1 - f(E_k)]$$

$$+ f(E_k)\ln f(E_k)\} ,   (45)$$

where

$$n_k = \frac{1}{2}\left[1 - \frac{\varepsilon_k - \mu}{E_k}[1 - 2f(E_k)]\right]   (46)$$

is the "hole density" with wave vector k at finite temperature. The second term in Eq. (45) is the energy lowering due to the interaction and the third term is just the usual entropy contribution. The free energy in the normal state is given by Eqs. (45) and (46) with $\Delta_k \rightarrow 0$ and $\mu \rightarrow \mu_n$, where μ_n is the chemical potential the system would have if it were in the normal state. We have computed $H_c(T)$ from Eq. (44), and in particular the deviation function;

$$D(T/T_c) = H_c(T)/H_c(0) - [1 - (T/T_c)^2]$$

which subtracts off the two-fluid-model result. For $t^h = 0.030$ eV, the discrepancy with weak-coupling BCS theory is very minor. Equations (42) and (43) determine the Ginzburg-Landau values of the coherence length and the upper critical magnetic field. As remarked earlier, the anisotropy in these properties is the same as in the penetration depth. Furthermore, the coherence lengths are very short within the model used here, for the reasons discussed earlier. In Fig. 19 we plot $|dH_{c2}^{\perp}(T)/dT|_{T_c}$ versus n, again normalized to the value at the density with the maximum T_c, $n_{max} = 0.037$, along with the extracted GL coherence length at $T = 0$, again normalized to the value at n_{max}. Note the monotonic behavior of these quantities despite the nonmonotonic behavior of T_c. It is clear that at large hole concentrations the coherence length is expected to diverge.

C. Thermodynamics and tunneling

Several aspects of the thermodynamics and tunneling have been discussed in Refs. 4 and 25 within this model. In Fig. 20 we plot $2\Delta_0/k_B T_c$ and $\Delta C(T_c)/C_N(T_c)$ versus hole density for the parameters indicated in the figure
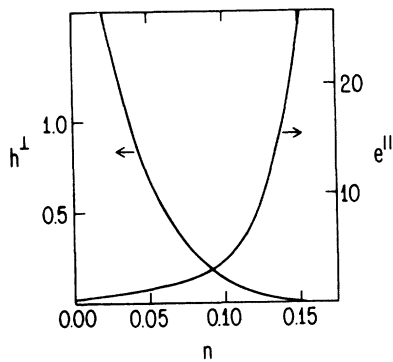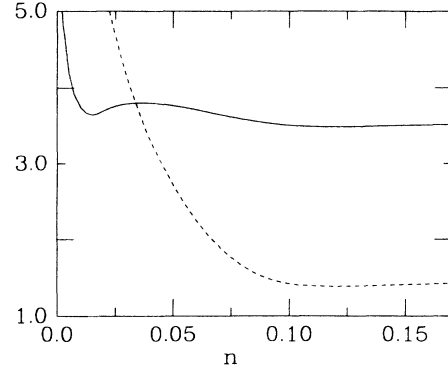

FIG. 20. Gap ratio $2\Delta_0/k_B T_c$ (solid line) and normalized specific-heat jump, $\Delta C(T_c)/C_N(T_c)$ (dashed line) vs hole concentration for $t_{\parallel}^h = 0.030$ eV, $\rho = 0.025$, $U = 5$ eV, and $K = (U + W)/2$ with maximum $T_c = 100$ K.

caption. At high densities the BCS weak-coupling results are always obtained. At low frequencies large deviations are obtained. As discussed in Ref. 11, large values of the gap ratio, $2\Delta_0/k_B T_c$ are obtained for narrower bandwidths than are displayed in Fig. 20. In the case illustrated, $t_{\parallel}^h = 0.03$ eV, so that large values of the gap ratio are achieved only at very low densities. Moreover, the specific-heat jump value increases substantially at low densities; this is, however, predominantly a normal-state effect, since $C_n(T_c) \ll \gamma_0 T_c$, where γ_0 is the zero-temperature Sommerfeld constant. This occurs because $T_c \gtrsim E_F$, which occurs within our model in the low-density limit. Unfortunately, this property is also one of the most difficult to measure experimentally, as it is generally not known how to separate the electronic contribution to the specific heat from the other contributions.

Tunneling has always been a very useful probe of superconductivity in the past. In the high-T_c oxides, tunneling studies have not been as successful. I-V characteristics showing a very well-defined gap have been presented,[1] but these are often not reproducible. For the most part, I-V characteristics always show states within the "gap," making the gap determination ambiguous. The normal-state tunneling results appear to display a *linearly increasing* background,[26] as a function of energy. These are, however, in an apparent conflict with the corresponding photoemission results,[27] which ought to, in principle at least, measure the same underlying density of states. We bypass this last issue, and in Fig. 21 show the *normalized I-V* characteristic in the superconducting state. For simplicity we have used a constant normal density of states, with $U = 5$ eV, $t^h = 0.03$ eV, and Δt and V adjusted so that the relation $K = (U + W)/2$ is maintained, with a maximum $T_c = 100$ K. The asymmetry in the density of states is clearly evident in Fig. 21. At temperatures approaching T_c there is an added component of asymmetry (of the same sign) due to the fact that the chemical potential is near the bottom of the band. The overall percentage asymmetry expected here is somewhat less than that reported in Ref. 4, because here we have included a nearest-neighbor repulsion, V, which causes a decrease in the slope of $\Delta(\varepsilon)$ versus ε, making the solu-

FIG. 19. Plot of $h^{\perp} \equiv T_c(n) \cdot dH_{c2}^{\perp}/dT(T_c, n)/100 \cdot dH_{c2}^{\perp}/dT(T_c, 0.037)$ (left-hand scale) and $e^{\parallel} \equiv \xi_{GL}^{\parallel}(0, n)/\xi_{GL}^{\parallel}(0, 0.037)$ vs n for the case $t_{\parallel} = 0.03$ eV, $\rho = 0.025$, $U = 5$ eV, $v = 1$, and Δt and $V_{\parallel}$ determined so that $K = (U + W)/2$ and maximum $T_c = 100$ K. The critical-field slopes and GL coherence lengths have been normalized to their respective values at $n = 0.037$, which is where the maximum T_c occurs. Within our model the reduced ratio, $H_{c2}(0)/T_c|H_{c2}'(T_c)|$ differs only slightly from the WHH (Ref. 23) value of 0.7 over the entire density range, so that the usual procedure for extracting coherence lengths from upper critical-field data is justified for qualitative estimates.
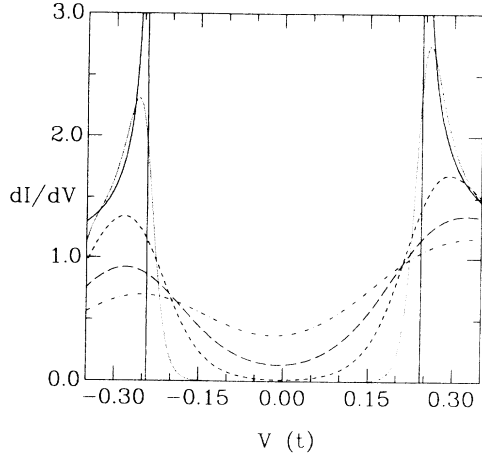
FIG. 21. dI/dV vs V for constant density-of-states model with $t^h=0.030$, $U=5$, and Δt and V chosen so that $K=(U+W)/2$ and maximum $T_c=100$ K. Plot is for $n=0.07$ ($T_c\sim93$ K) and for temperatures $T/T_c=0$ (solid), 0.1 (dotted), 0.3 (short dashed), 0.5 (long dashed), and 0.7 (dot dashed). Positive voltage indicates that holes are injected into the sample.

tion more BCS like, i.e., symmetric. To illustrate this, we have plotted in Fig. 22 the gap function versus energy for various fillings for two sets of parameters, one with $V\neq0$ (dashed lines) and one with $V=0$ (solid lines). As expected, those with $V=0$ have slopes of larger magnitude, thus enhancing the asymmetry. The degree of asymmetry, X, is given at $T=0$ by[28]

$$X=2\frac{\Delta_m}{D/2}\frac{1}{\{1+[\Delta_m/(D/2)]^2\}^{1/2}}(100\%)\ . \qquad (47)$$

Actual values are given in the figure caption. We have adjusted Δt so that the maximum T_c remains 100 K. The T_c versus n curves for the two cases are then very similar. As the hole concentration is increased, the asymmetry is further reduced in the case when $V\neq0$, since a larger Δt is required and so the effective bandwidth increases, causing X to decrease more rapidly as n increases. Another important feature that is visible in Fig. 21 is that the "gap," as determined visually from the peaks in the I-V characteristic, seems to be *increasing* as the temperature increases towards T_c. This is simply an artifact of the convolution of the density of states with a Fermi function derivative. In actual fact, the gap is decreasing as a function of temperature in a BCS-like manner. We have discussed elsewhere[11] cases where in fact the gap remains fairly constant as a function of temperature right up to $T=T_c$. However, thermal smearing makes it difficult to differentiate between the two cases on the basis of curves as in Fig. 21.

Several other properties in the superconducting state have been calculated. The spin susceptibility in a uniform field is given in our model by the usual expression[29]

$$\chi_0=-2\mu_0^2\sum_k\frac{\partial f}{\partial E_k} \qquad (48)$$

with μ_0 the Bohr magneton. Below T_c it vanishes exponentially due to the existence of a gap over the entire Fermi surface, closely following BCS behavior. This implies that the contribution of the holes described by our model Hamiltonian to measured Knight shifts should decrease exponentially as T goes to zero. In Fig. 23 we illustrate the normalized Knight shift as a function of temperature for three different hole concentrations. The deviation from the weak-coupling BCS result is largest at small hole densities. Experimentally, a rapid decrease of Knight shifts is observed below T_c in high T_c oxides.[30]

The nuclear-spin relaxation rate in isotropic superconductors is usually assumed to be proportional to[29]

$$R=\int_{\Delta_0}^{\infty}dE\ g_s(E)^2\left[1+\frac{\Delta^2}{E^2}\right]f(E)[1-f(E)] \qquad (49)$$

and it gives rise to a peak (Hebel-Slichter peak) in the relaxation rate below T_c due to the divergence in the superconducting density of states $g_s(E)$ at the gap edge. In our model such a peak in R is obtained below T_c. Its effect on the relaxation rate of Cu and O nuclei, however, will be modulated by form factors and hyperfine coupling constants[31] and it is conceivable that the effect is consider-
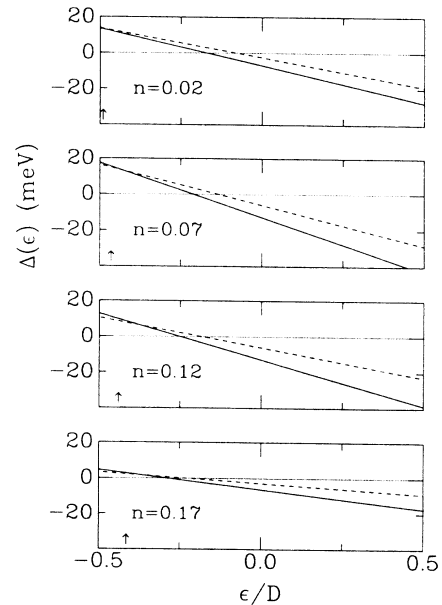

FIG. 22. Gap function, $\Delta(\varepsilon)=\Delta_m(c-\varepsilon/D/2)$ vs ε/D, for various values of the hole concentration, $n=0.02$, 0.07, 0.12, and 0.17. The dashed lines are for the parameters of Fig. 20, i.e., with V nonzero. The solid lines were obtained from solutions for the case $V=0$. In this case, $\Delta t=0.188$ eV was chosen to give a maximum $T_c=100$ K. The T_c vs n curves for the two cases are very nearly the same. The slopes of the gap functions in the first case ($V\neq0$) are smaller in magnitude (more "BCS-like") than when $V=0$, and so the expected asymmetry will be smaller. The actual values of the resulting asymmetries at $T=0$ are 30% (21%) for $n=0.02$, 35% (18%) for $n=0.07$, 24% (10%) for $n=0.12$, and 9% (3%) for $n=0.17$, for $V=0$ ($V\neq0$).
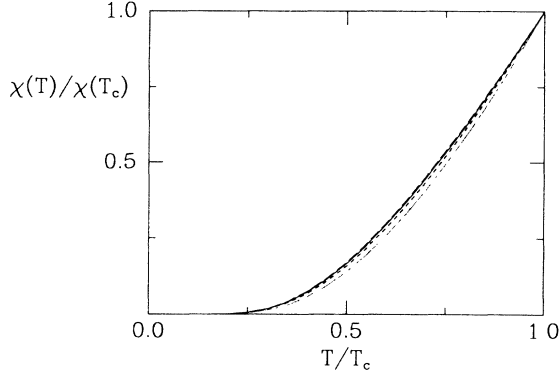
FIG. 23. Plot of normalized Knight shift, $\chi(T)/\chi(T_c)$ as a function of reduced temperature, T/T_c. The solid line is for the weak-coupling BCS result. The other curves have been calculated for $t_\parallel^h = 0.03$ eV, $U = 5$ eV, with $\rho = 0.025$ and $v = 1$. Δt and $V_\parallel$ have been adjusted for $T_c^{\max} = 100$ K. The densities are $n = 0.02$ (dotted), $n = 0.08$ (short dashed) and $n = 0.14$ (long dashed). The deviations are largest for small hole densities.

ably suppressed. Conflicting experimental reports exist[32] on the question of the existence of a peak in the relaxation rate of ^{17}O below T_c.

V. PAIR WAVE FUNCTION AND COHERENCE LENGTH

It is interesting to examine the shape of the pair wave function in our model. It was shown in Ref. 4 that some amplitude always exists in the pair wave function for "on-site" pairs but that the largest amplitude is for "nearest-neighbor" pairs, increasingly so for larger U. Here we consider the effect of anisotropy as well as the density dependence. Given the solution to the Eqs. (6), one can calculate the pair wave function amplitude in real space:[4]

$$f(\mathbf{R}) = \frac{\langle c_{r\downarrow} c_{0\uparrow} \rangle}{\langle c_{0\downarrow} c_{0\uparrow} \rangle} \qquad (50)$$

with

$$\langle c_{R\downarrow} c_{0\uparrow} \rangle = \frac{1}{N} \sum_k \Delta_k \frac{1 - 2f(E_k)}{2E_k} e^{i\mathbf{k}\cdot\mathbf{R}} . \qquad (51)$$

Equations (6) have been solved below T_c through numerical computation of the momentum sums involved. In Fig. 24(a) we plot $f(\mathbf{R})$ versus R_x, with $R_y = R_z = 0$, and in Fig. 24(b) we plot $f(\mathbf{R})$ versus R_z, with $R_x = R_y = 0$ for the parameters discussed in the figure caption. Comparison of the two figures shows clearly that the wave function is far more extended in the plane than normal to the plane. An effective measure of this extension is the mean-square radius of a hole pair:

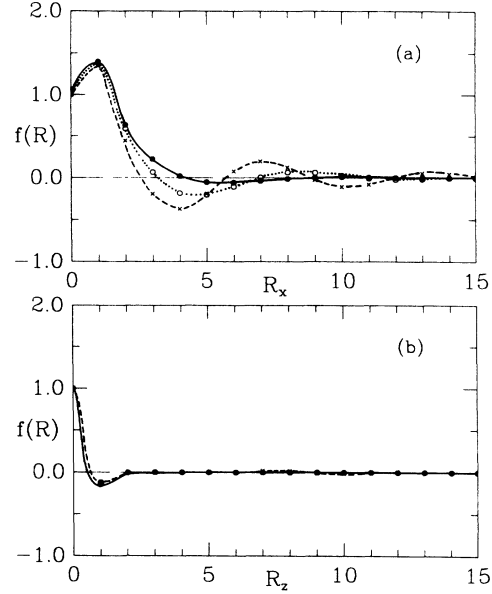$$\langle R_v^2 \rangle = \frac{\sum\limits_R f^*(R) R_v^2 f(R)}{\sum\limits_R f^*(R) f(R)} . \qquad (52)$$

FIG. 24. Plot of (a) $f(\mathbf{R})$ vs R_x and (b) $f(\mathbf{R})$ vs R_z, for three values of the hole concentration, $n = 0.05$ (●), $n = 0.10$ (○), and $n = 0.15$ (×). We have used $t_\parallel^h = 0.03$ eV, $\rho = 0.1$, and $U = 5$ eV (see Table I). The functions plotted are at $T = 0$, and correspond to values of T_c of 98 K, 61 K, and 13 K for $n = 0.05$, 0.10, and 0.15, respectively. Note that the wave amplitude barely changes in the z direction for the three hole concentrations. The coherence lengths in units of lattice spacing are $\xi_\parallel = 1.3$ ($\xi_\perp = 0.19$) $\xi_\parallel = 3.1$ ($\xi_\perp = 0.42$), and $\xi_\parallel = 19$ ($\xi_\perp = 2.3$) for $n = 0.05$, 0.10, and 0.15, respectively.

We define the coherence length to be

$$\xi_v \equiv \langle R_v^2 \rangle^{1/2} , \qquad (53)$$

which differs by a factor of $2\sqrt{2}/\pi \approx 0.9$ from the BCS definition. At $T = 0$, Eqs. (50), (51), and (52) combine to give

$$\xi_v^2 = \frac{(1/N) \sum\limits_k |\nabla_k(\Delta_k/2E_k)|_v^2}{(1/N) \sum\limits_k (\Delta_k/2E_k)^2} . \qquad (54)$$

Computations of ξ_v^2 are much simpler within the "isotropic" model defined by Eq. (19). In Fig. 25 we show a curve giving this coherence length in the x direction as a function of hole concentration for $t_\parallel^h = 0.03$ eV, $U = 5$ eV, and $\rho = 0.1$, using the isotropic kernel, Eq. (19). Δt and $V_\parallel$ are determined from the constraints $K = (U + W)/2$ and maximum $T_c = 100$ K. Also shown are a few points illustrating the full solution incorporating the anisotropic gap, Eq. (7), for the parameters given in Table I. As has already been emphasized, the gap anisotropy has essentially no effect on the result. Also shown is the Ginzburg-Landau coherence length, as determined through the GL equations along with microscopic calculations of the London penetration depth and the thermodynamic critical field (see Sec. IV). It is clear that both
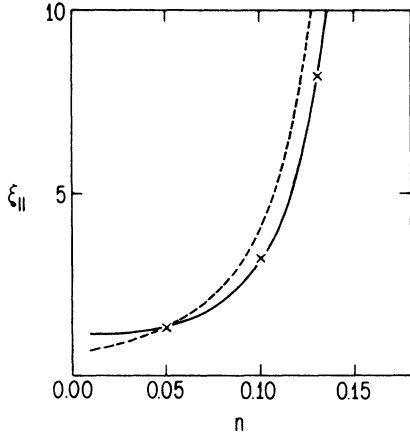
FIG. 25. Plot of ξ_x vs hole concentration for $t_\parallel^h = 0.030$ eV, $\rho = 0.1$, $U = 5$ eV, within the isotropic model (solid line). The points marked with an "×" are values determined from the fully anisotropic calculation (see Table I for parameter values). Also shown is the Ginzburg-Landau coherence length (dashed line) as determined from the penetration depth and thermodynamical critical field.

are in qualitative agreement, though quantitative differences up to factors of 2 can occur. As $T \rightarrow T_c$, the Ginzburg-Landau coherence length diverges; the one defined by Eq. (53) does not. This is so because the Ginzburg-Landau coherence length takes into account that the superconducting fraction approaches zero as $T \rightarrow T_c$. On the other hand, the BCS coherence length defined by Eq. (53) gives the coherence length *for* the superconducting fraction. We have found that this latter coherence length is nearly constant over the entire temperature range up to T_c.

In Fig. 26(a) we plot the anisotropy in the coherence length for the case shown in Fig. 25. While there is a distinct quantitative difference between the anisotropy of the BCS and GL coherence length at low fillings, the anisotropy ratios become equal at high filling, where the weak-coupling limit is achieved. In this limit Eq. (54) gives

$$\frac{\xi_\parallel}{\xi_\perp} = \left[\frac{g_\parallel(\mu)}{g_\perp(\mu)} \right]^{1/2} , \tag{55}$$

which is identical to that given by Eq. (38) along with (42).

The strong-coupling limit is discussed in Appendix B. In that case the pairing amplitudes are nonzero for on-site and nearest-neighbor pairs only. The analysis in that appendix yields $\xi_\parallel/\xi_\perp = \rho^{-1}$ in the dilute limit. In Fig. 26(b), we plot $\xi_\parallel/\xi_\perp$ and $\xi_{GL}^\parallel/\xi_{GL}^\perp$ versus n for the case $t_\parallel^h = 0.001$ eV, $U = 5$ eV, and $\rho = 0.1$. Again, we have used the isotropic kernel and chosen Δt and $V_\parallel$ such that $K = (U + W)/2$ and maximum $T_c = 100$ K. Clearly, the weak-coupling limit is achieved at high densities once again. At low densities, the two results differ considerably; the BCS coherence length anisotropy approaches
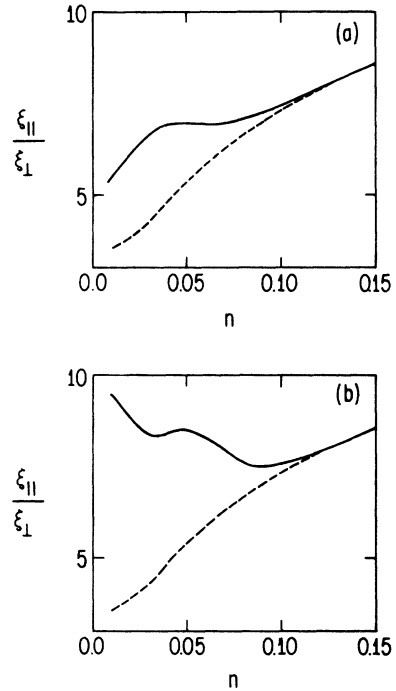

FIG. 26. (a) Plot of BCS coherence lengths anisotropy ratio (solid line) for same parameters as Fig. 25. Also shown is the GL coherence length (dashed line). They agree in the weak-coupling limit at high densities. In (b) the same ratios are plotted for $t_\parallel^h = 0.001$ eV, so that the strong-coupling limit is achieved in the dilute limit (weak coupling is still achieved at high densities). The discrepancy at low densities is significant. [$\xi_\parallel/\xi_\perp = \rho$ and $\xi_{GL}^\parallel/\xi_{GL}^\perp = \sqrt{\rho}$].

$1/\rho$ as $n \rightarrow 0$, as determined analytically, while the GL anisotropy approaches $1/\sqrt{\rho}$, as for the case $t_\parallel^h = 0.03$ eV. This latter result is simply the effective-mass approximation, as remarked earlier. The reason for the discrepancy is that the GL coherence length is calculated from the penetration depth given by expression (32). As remarked there, this expression is based on single-particle hops, whereas in the strong-coupling limit pair hopping is dominant. Thus, in Fig. 25, for example, at low filling the BCS coherence length exceeds the GL coherence length, so that using Eq. (42) we expect the actual penetration depth (that is, one which includes pair hopping processes in determining screening currents) to be smaller than the one actually calculated from Eq. (36), bringing the values in closer agreement with experiment. Furthermore, as is clearly indicated by Fig. 26(b), the monotonic increase in anisotropy as a function of filling no longer holds in the strong-coupling regime.

VI. DISCUSSION

We have discussed here various properties of a model for superconductivity where pairing is driven by the enhancement of the hopping amplitude of a hole by the

presence of another hole nearby. In particular, we have examined new features that appear for a three-dimensional anisotropic band structure, as appropriate for the layered oxide superconductors, and taken into account the effects associated with the single-particle hopping renormalization that necessarily occurs with this pairing interaction.

It is important to emphasize two features of our model. First is its remarkable simplicity. Due to the particular nature of the model, the BCS solution is not just a mathematical exercise that may differ considerably from its exact solution, as occurs with other models. Contrary to some statements made in the conclusion of our previous study,[4] we now believe that the BCS solution of this model is close to being exact in the physical parameter range. The reason is that the system is always dilute when it is superconducting, and the strong-coupling regime occurs only when it is extremely dilute so that BCS theory remains applicable.[11]

The second feature we wish to emphasize is that within our model the calculated superconducting properties are fairly insensitive to the parameters used. As discussed in the text, given the constraint Eq. (12) for the interactions and reasonable band widths as inferred from experiments, little room remains for changing the results by varying parameters like the on-site U or the anisotropy. Unless a major modification of the model is invoked, the results shown in this paper should span the regime of behavior that includes the high-T_c oxides.

As a consequence of these two features, the predictions of this model are definite. Should experiments convincingly demonstrate, for example, that comparable changes in T_c are obtained in changing either in-plane or interplane atomic distances, or that the tunneling asymmetry is of opposite sign as we predict, then the model is clearly incorrect. Conversely, experimental verification of the various trends discussed here, particularly as a function of hole concentration, should provide strong support for the model as well as further constrain the values of the parameters that enter in the model Hamiltonian.

We conclude by summarizing the main features and trends discussed in this paper and the experimental status on each point to our knowledge.

(1) *Gap anisotropy.* As discussed, in this model the gap is essentially constant over the Fermi surface except for possible small deviations (less than 5%) that give a measure of the importance of extended Coulomb repulsion. High-resolution photoemission experiments should be able to address this question in the near future; to our knowledge, the existing experimental information is consistent with an isotropic gap. Within our model larger gap anisotropies would only be obtained with an unphysically large value of the nearest-neighbor Coulomb repulsion V and/or unphysically large anisotropies in V, and a magnitude of the interplane hopping that would be inconsistent with a variety of other experiments.

(2) T_c *versus concentration dependence.* Although there is still some debate on the issue, several groups[6-9] have by now convincingly demonstrated that a maximum in T_c occurs as a function of hole concentration and that T_c goes to zero when the number of holes becomes too large,

while at the same time the system becomes increasingly metallic. This behavior is the most characteristic feature of the hole pairing mechanism. Our single-band model appears to rule out superconductivity with the required T_c's at hole concentrations larger than about 0.2 per plane oxygen (0.4 per plane Cu).

(3) *Pressure derivative of* T_c. We can only make definite predictions about the change in T_c with lattice spacing. Thus, in experiments where the change in T_c with pressure is studied one should at the same time attempt to determine whether charge transfer occurred under pressure between different parts of the system, for example, by Hall coefficient measurements. In addition, the change in lattice constant in the plane and perpendicular to the plane directions under pressure should be measured. Our model predicts a ratio of change in T_c with interplanar versus intraplanar atomic distance of about ρ^2, with ρ the hopping anisotropy. There is also a definite trend with hole concentration, with the pressure derivatives increasing with the number of holes. These two predictions appear to be inconsistent with recently reported experimental results.[7,19] If a negative pressure derivative in the z direction for low hole concentration is observed it will constrain the allowed values of our hopping parameter $t_{\parallel}^h$.

(4) *Coherence length versus doping.* Our model predicts the coherence length to monotonically increase with doping, diverging at the density where $T_c \to 0$. This behavior should be evident in critical-field measurements, but has to our knowledge not yet been systematically studied. The magnitude of the coherence length for small hole concentrations should also provide information on the size of our hopping parameter $t_{\parallel}^h$. A further consequence of this behavior is that a crossover from type-II to type-I superconductivity will occur at the highest hole concentration as $T_c \to 0$. This is most likely to be achieved in the $La_{1-x}Sr_xCuO_4$ system.

(5) *Effective mass versus doping.* The single-particle effective mass m^* is inversely proportional to the hopping amplitude and thus should decrease monotonically with doping [Eq. (10)]. This should be manifest in various normal-state properties. Indeed, the observed rapid decrease in the measured resistivity with doping clearly indicates this behavior. Optical experiments should also be able to infer the dependence of effective mass on doping through the weight of the Drude peak in the low-frequency conductivity $\sigma(\omega)$. However, interpretation of experiments up to now have been complicated by the presence of non-Drude-like absorption.[33] Below T_c the decrease in effective mass with doping should be observable in measurements of the London penetration depth, but presently available data do not seem to confirm this behavior.[34] The situation below T_c is also complicated by the fact that the hopping interaction Δt will also contribute to the effective mass. As discussed in Sec. IV, for low hole densities Δt gives the dominant contribution to the hole hopping amplitude, which was not taken into account in our calculation of λ. This is not the case above T_c, as pairs dissociate and the contribution of Δt to the hole propagation is negligible. The rate of change of

effective mass with doping should provide direct information on the magnitude of the parameter Δt through Eq. (10).

(6) *Anisotropy in penetration depth and critical field.* Both the anisotropy of the penetration depth and critical field are determined by the hopping anisotropy ρ. In weak coupling (large hole densities) they are given by the usual Ginzburg-Landau expressions. For low hole densities (strong coupling) the anisotropy in the coherence length should be somewhere between $\sqrt{\rho}$ and ρ, depending on the value of the parameter $t_\parallel^h$. We have not calculated the penetration depth in strong coupling but expect that it would follow the corresponding behavior.

(7) *Tunneling asymmetry.* The magnitude of the tunneling asymmetry should provide an upper bound for the value of the nearest-neighbor repulsion V in our model. The density dependence of the asymmetry should approximately follow the density dependence of T_c, as discussed elsewhere.[28] The sign is universal, larger dI/dV corresponding to a negatively biased sample.

(8) *Gap ratio.* The gap ratio should decrease with hole doping, being larger than the BCS values at low hole densities. Large values of the gap ratio suggest small values of the parameter $t_\parallel^h$, as seen from the results in Ref. 11. For intermediate values of $t_\parallel^h$ (e.g., 0.03 eV) the gap ratio is BCS like except at the very lowest hole densities (see Fig. 20).

(9) *Specific-heat jump.* It should decrease with hole doping, being somewhat larger than the BCS value 1.43 at low hole densities. It is unlikely that this quantity could be determined accurately enough to be useful in further constraining the parameters in our model.

(10) *Other properties.* The temperature dependence of London penetration depth and thermodynamic critical field follow closely the BCS behavior. The contribution to the Knight shift due to the holes in our model should decrease exponentially at low temperatures in the usual way as the gap opens up. This is consistent with existing experiments.[30] Above T_c no pairs exist in our model[11] so that large Knight shifts are expected, as observed. The question on the existence of a Hebel-Slichter peak in the NMR relaxation rate below T_c is unclear. If an on-site coupling exists between the oxygen holes described by our model and the oxygen nuclear spin, our model necessarily implies such a peak in the ^{17}O relaxation rate. However, if the dominant hyperfine coupling of the ^{17}O nuclear spin is to nearest-neighbor Cu spins[31] the behavior could be very different and lies outside the model discussed here. To our knowledge, experimentally the presence or absence of a peak in the ^{17}O NMR relaxation rate is still open.

As emphasized in the Introduction, we have not addressed in this paper the problem of the disappearance of the antiferromagnetic order as the high-T_c oxides are doped, nor the role of the copper $d_{x^2-y^2}$ orbitals. These features are important for a complete understanding of the physics of high-T_c oxides and should be incorporated in a model together with the physics described by the Hamiltonian Eq. (1). We do not believe, however, that the main conclusions already discussed would be changed by such a description. In the "electron-doped" oxides,[35] while we expect the physics of superconductivity to still be dominated by induced oxygen holes described by the Hamiltonian Eq. (1) the detailed behavior may be somewhat different due to the presence of a larger number of electronlike carriers at the Fermi surface.[36] These questions should be addressed in the future.

ACKNOWLEDGMENTS

APPENDIX A: SOLUTION OF THE BCS EQUATIONS

We outline here the method of solution to Eq. (6), using the ansatz (7). Equation (6a) is rewritten:

$$\Delta_k = -\frac{1}{N}\sum_{k'}\left[U+\frac{K}{4t_\parallel}(\varepsilon_k+\varepsilon_{k'})+W\rho_{kk'}\right]\frac{\Delta_{k'}}{2(\varepsilon_{k'}-\mu)}[1-2f(\varepsilon_{k'}-\mu)] , \tag{A1}$$

where

$$\rho_{kk'}=\tfrac{1}{2}(\cos k_x\cos k_x'+\cos k_y\cos k_y'+v\,\cos k_z\cos k_z') \tag{A2}$$

and $v \equiv V_\perp/V_\parallel$, $K=8\alpha t_\parallel$, and $W=4V_\parallel$. The momenta k_x' and k_y' are equivalent in Eq. (A1), so that Eq. (A2) can be rewritten:

$$\rho_{kk'}=\left[-\frac{\varepsilon_k}{4t_\parallel}\right]\left[-\frac{\varepsilon_{k'}}{4t_\parallel}\right]+\frac{\rho}{2}\cos k_z'\left[-\frac{\varepsilon_k}{4t_\parallel}\right]+\cos k_z\left\{\frac{\rho}{2}\left[-\frac{\varepsilon_{k'}}{4t_\parallel}\right]+\left[\left[\frac{\rho}{2}\right]^2+\frac{v}{2}\right]\cos k_z'\right\} . \tag{A3}$$

With the ansatz (7), we obtain three equations to be solved simultaneously for T_c, c', and c:

$$c'=W\left\{\frac{\rho}{2}(cI_1+I_2-c'J_1)+\left[\left[\frac{\rho}{2}\right]^2+\frac{v}{2}\right](cJ_0+J_1-c'L_0)\right\} , \tag{A4a}$$

$$-c=U(cI_0+I_1-c'J_0)-K(cI_1+I_2-c'J_1) , \tag{A4b}$$

$$1 = K(cI_0 + I_1 - c'J_0) - W(cI_1 + I_2 - c'J_1) - W\frac{\rho}{2}(cJ_0 + J_1 - c'L_0) \; . \tag{A4c}$$

Here

$$I_l \equiv \int_{-D/2}^{D/2} d\varepsilon \, g_0(\varepsilon) \left[-\frac{\varepsilon}{4t_\parallel} \right]^l \frac{1 - 2f(\varepsilon - \mu)}{2(\varepsilon - \mu)} \; , \tag{A5a}$$

$$J_l \equiv \int_{-D/2}^{D/2} d\varepsilon \, g_1(\varepsilon) \left[-\frac{\varepsilon}{4t_\parallel} \right]^l \frac{1 - 2f(\varepsilon - \mu)}{2(\varepsilon - \mu)} \; , \tag{A5b}$$

and

$$L_l \equiv \int_{-D/2}^{D/2} d\varepsilon \, g_2(\varepsilon) \left[-\frac{\varepsilon}{4t_\parallel} \right]^l \frac{1 - 2f(\varepsilon - \mu)}{2(\varepsilon - \mu)} \; , \tag{A5c}$$

where

$$g_j(\varepsilon) \equiv \frac{1}{N} \sum_{k'} \cos^j k_z' \delta(\varepsilon - \varepsilon_{k'}) \tag{A6}$$

$$= \frac{1}{2\pi^2 t_\parallel} \int_0^1 dx \, \cos^j(\pi x) K \left[1 - \left| \frac{\varepsilon}{4t_\parallel} - \frac{\rho}{2} \cos\pi x \right|^2 \right] \Theta \left[1 - \left| \frac{\varepsilon}{4t_\parallel} - \frac{\rho}{2} \cos\pi x \right| \right] , \tag{A7}$$

where $K(x)$ is the complete elliptic integral of the first kind. In practice, we eliminate c and c' through Eqs. (A4a) and (A4b), and iterate the one equation (A4c) to convergence:

$$1 = \psi[T_c, c(T_c), c'(T_c)] \; , \tag{A8}$$

where ψ is a complicated functional form that follows simply from Eqs. (A4). We have also solved Eqs. (A4) below T_c, where we have generalized Eqs. (A5) to temperatures below T_c, and used three-dimensional k sums to compute the resulting integrals.

As discussed in the text, when $\rho = 0$, the anisotropy in the gap vanishes, regardless of the values of $v \equiv V_\perp / V_\parallel$. This is readily seen from Eq. (A4a), along with the fact that $g_1(\varepsilon) \equiv 0$, as follows trivially from Eq. (A7). When cubic symmetry is present, or one invokes the isotropic approximation mentioned in Sec. II, then the equations simplify significantly. One obtains the T_c equation:[3]

$$1 = 2KI_1 - WI_2 - UI_0 + (K^2 - WU)(I_0 I_2 - I_1^2) \; , \tag{A9}$$

where

$$K = 2z\alpha t_\parallel \; , \tag{A10a}$$

$$W = zV_\parallel \; , \tag{A10b}$$

and

$$I_l = \int_{-D/2}^{D/2} d\varepsilon \, g(\varepsilon) \left[-\frac{\varepsilon}{D/2} \right]^l \frac{1 - 2f(\varepsilon - \mu)}{2(\varepsilon - \mu)} \; . \tag{A11}$$

Here, z is the number of nearest neighbors, $g(\varepsilon)$ is the electron density of states, $D \equiv 2zt_\parallel$ is the bandwidth, and $\varepsilon = \varepsilon^0(1 + \alpha n)$ is the renormalized single-particle energy. We have assumed $t_\perp = t_\parallel$ and $V_\perp = V_\parallel$ in Eqs. (A9)–(A11). The ansatz for the gap is $\Delta(\varepsilon) = \Delta_m[c - \varepsilon/(D/2)]$.

In the weak-coupling limit, Eqs. (A9) and (A11) can be solved analytically.[3,4] In Ref. 3 the solution with non-

constant density of states was discussed but a term was omitted, so that we discuss here the solution for completeness. We assume an arbitrary density of states function $g(\varepsilon)$, with $-D/2 \leq \varepsilon \leq D/2$. The number of holes for given chemical potential is

$$n = 2 \int_{-D/2}^{\mu} d\varepsilon \, g(\varepsilon) \tag{A12}$$

and we define also an "effective" number of holes:

$$\bar{n} = 1 + \mu/(D/2) \; , \tag{A13}$$

which coincides with n for constant density of states. For given chemical potential we write the density of states as

$$g(\varepsilon) = g(\mu)[1 + \delta_\mu(\varepsilon)] \tag{A14}$$

so that the relation between n and $\bar{n}$ is

$$n = Dg(\mu)\bar{n} - 2g(\mu) \int_{-D/2}^{\mu} d\varepsilon \delta_\mu(\varepsilon) \; . \tag{A15}$$

Defining the parameters:

$$k = Kg(\mu) \; , \tag{A16a}$$

$$w = Wg(\mu) \; , \tag{A16b}$$

$$u = Ug(\mu) \; , \tag{A16c}$$

the result for T_c within BCS approximation $[T_c / (nD) \ll 1]$ is

$$T_c = \frac{e^\gamma}{\pi} D \sqrt{\bar{n}(2 - \bar{n})} e^{-a/b} \tag{A17}$$

$$a = a_0 + \delta a \; , \tag{A18a}$$

$$b = b_0 + \delta b \; , \tag{A18b}$$

with

$$a_0 = 1 + 2k(1 - \bar{n}) - w(1 - 3\bar{n} + \tfrac{3}{2}\bar{n}^2) + (k^2 - wu)(1 - \bar{n})^2 \tag{A19a}$$

$$b_0 = 2k(1-\bar{n}) - w(1-\bar{n})^2 - u + (k^2 - wu)\left[1 - \bar{n} + \frac{\bar{n}^2}{2}\right]$$

(A19b)

and

$$\delta a = 2[k - w(1-\bar{n})]\delta A_1 + w\delta A_2$$
$$+ (k^2 - wu)[2(1-\bar{n})\delta A_1 + \delta A_1^2] - (b_0 + \delta b)\delta A_0 ,$$

(A20a)

$$\delta b = (k^2 - wu)\delta A_2$$

(A20b)

with

$$\delta A_l = \left[\frac{2}{D}\right]^l \int_{-D/2}^{D/2} d\varepsilon \frac{\delta_\mu(\varepsilon)}{2}(\varepsilon - \mu)^{l-1}\mathrm{sgn}(\varepsilon - \mu) .$$

(A21)

[The last term in Eq. (A20a) was omitted in Ref. 3.] For example, for the particular case of a linear density of states;

$$g(\varepsilon) = \frac{1}{D}\left[1 + \frac{a_1\varepsilon}{D/2}\right] ,$$

(A22)

we have

$$\delta_\mu(\varepsilon) = b_1\frac{\varepsilon - \mu}{D/2}$$

(A23)

with

$$b_1 = \frac{a_1}{1 + a_1\mu/(D/2)}$$

(A24)

and Eq. (A21) yields

$$\delta A_0 = b_1(1-\bar{n}) ,$$

(A25a)

$$\delta A_1 = b_1\left[1 - \bar{n} + \frac{\bar{n}^2}{2}\right] ,$$

(A25b)

$$\delta A_2 = \tfrac{1}{3}b_1(1-\bar{n})[3 + (1-\bar{n})^2] ,$$

(A25c)

and from Eq. (A15)

$$n = \bar{n} - \frac{a_1}{2}\bar{n}(2-\bar{n}) ,$$

(A26)

which is simply solved for $\bar{n}(n)$. We have verified the correctness of these equations by comparison of the analytic results with the numerical solution of the BCS equations.

The gap ratio in the weak-coupling limit is simply obtained in the isotropic case. Equation (A11) below T_c becomes

$$I_l = \int_{-D/2}^{D/2} d\varepsilon\, g(\varepsilon)\left[-\frac{\varepsilon}{D/2}\right]^l \frac{1 - 2f(E(\varepsilon))}{2E(\varepsilon)}$$

(A27)

with

$$E(\varepsilon) = [(\varepsilon - \mu)^2 + \Delta^2(\varepsilon)]^{1/2} ,$$

(A28)

$$\Delta(\varepsilon) = \Delta_m\left[c - \frac{\varepsilon}{D/2}\right] ,$$

(A29)

and at $T = 0$

$$I_l = \int_{-D/2}^{D/2} d\varepsilon\, g(\varepsilon)\left[-\frac{\varepsilon}{D/2}\right]^l \frac{1}{2\sqrt{(\varepsilon - \mu)^2 + \Delta^2(\varepsilon)}} .$$

(A30)

To lowest order in Δ_m/D the quasiparticle gap Δ_0 is given simply by $\Delta(\mu)$. By expanding $\Delta(\varepsilon)$ in Eq. (30) around $\Delta(\mu)$ one obtains

$$\Delta_0 = D\sqrt{\bar{n}(2-\bar{n})}e^{-a/b} + O((\Delta_m/D)^2)$$

(A31)

so that the gap ratio is

$$\frac{2\Delta_0}{k_B T_c} = 3.53 + O((\Delta_m/D)^2)$$

(A32)

as in the usual BCS case.

APPENDIX B: THE STRONG-COUPLING LIMIT

We discuss here the properties of our model in the limit where the single-particle hopping amplitudes $t_\parallel$ and $t_\perp$ go to zero. The isotropic case is discussed in Ref. 11. The wave function for a single pair is a linear combination of the wave functions:

$$|\psi_p\rangle = \frac{1}{\sqrt{N}}\sum_i |\uparrow\downarrow\rangle_i ,$$

(B1a)

$$|\psi_z\rangle = \frac{1}{\sqrt{N}}\sum_z |s\rangle_z ,$$

(B1b)

$$|\psi_{xy}\rangle = \frac{1}{\sqrt{2N}}\left[\sum_x |s\rangle_x + \sum_y |s\rangle_y\right] ,$$

(B1c)

where $|\uparrow\downarrow\rangle_i$ denotes a doubly occupied site and $|s\rangle_\mu$ a singlet on a bond labeled by μ. The sums in Eqs. (B1b) and (B1c) are over all bonds in a given direction (x, y, or z). For $t_\parallel = t_\perp = 0$, the Hamiltonian Eq. (1) has zero matrix elements between a state in the subspace spanned by the states in Eq. (B1) and any other state in the Hilbert space. We construct then the Hamiltonian matrix in that subspace:

$$H = \begin{bmatrix} U & -K/2 & \frac{K}{\sqrt{8}}\rho \\ -K/2 & W/4 & 0 \\ \frac{K}{\sqrt{8}}\rho & 0 & \frac{vW}{4} \end{bmatrix}$$

(B2)

and the binding energy of the pair, E_b, is minus the lowest eigenvalues of this matrix, E_0. It satisfies the cubic equation

$$(E_b+U)\left[E_b+\frac{W}{4}\right]\left[E_b+\frac{W}{4}v\right]-\frac{K^2}{4}\left[E_b+\frac{W}{4}v\right]-\frac{K^2v^2}{8}\left[E_b+\frac{W}{4}\right]=0 , \tag{B3}$$

which for the particular case $v=1$ considered in this paper simplifies to a quadratic equation:

$$(E_b+U)\left[E_b+\frac{W}{4}\right]-\frac{K^2}{4}\left[1+\frac{\rho^2}{2}\right]=0 \tag{B4}$$

with solution given in Eq. (28) of the text. The criterion on the parameters to obtain binding in this limit is obtained from Eq. (B3) by setting $E_b=0$ as

$$K^2 > \frac{v}{v+\rho^2/2}UW , \tag{B5}$$

which reduces both for $v=1$ and for $\rho=0$ to the criterion for binding in the isotropic strong-coupling limit $K^2 > UW$. (Note that for $\rho,v=1$ we should redefine our couplings as $\bar{K}=\frac{3}{2}K$ and $\bar{W}=\frac{3}{2}W$ to obtain the criterion in the usual form.) If there is no hopping in the third direction the nearest-neighbor repulsion in the third direction has no effect, as noted previously. Note also that for $v\rightarrow 0$ binding occurs for arbitrarily small K, as the pairs arrange themselves to lie predominantly on bonds pointing in the z direction.

Alternatively, Eq. (B3) can be derived from the BCS Eqs. (A4). In the limit where the single-particle hopping goes to zero we obtain for the quantities defined in Eq. (A5):

$$I_1=J_0=0 , \tag{B6a}$$

$$I_2=\frac{I_0}{4}\left[1+\frac{\rho^2}{2}\right] , \tag{B6b}$$

$$J_1=-\frac{\rho I_0}{4} , \tag{B6c}$$

$$L_0=\frac{I_0}{2} , \tag{B6d}$$

and substitution in Eq. (A4) yields

$$\frac{c}{I_0}=-Uc+\frac{K}{4}\left[1+\frac{\rho^2}{2}\right]+\frac{K\rho}{4}c' , \tag{B7a}$$

$$\frac{1}{I_0}=Kc-\frac{W}{4} , \tag{B7b}$$

$$\frac{c'}{I_0}=-\frac{W}{4}c'v+\frac{W}{8}\rho(1-v) . \tag{B7c}$$

In the dilute limit we have

$$I_0=\frac{1}{2|\mu|}=\frac{1}{E_b} \tag{B8}$$

and from Eqs. (B7b) and (B7c) we obtain

$$c=\frac{E_b+W/4}{K} , \tag{B9a}$$

$$c'=\frac{(W/8)\rho(1-v)}{E_b+(W/4)v} , \tag{B9b}$$

and substitution in Eq. (B7a) leads directly to the equation for the binding energy (B3) by using Eq. (B8). The gap in the dilute strong-coupling limit is simply $E_b/2$, and thus isotropic. Note also that the gap function Δ_k [Eq. (7)] becomes isotropic in the strong-coupling limit if $v=1$ [Eq. (B9b)].

The parameters c and c' are directly related to the amplitudes of the different components of the pair wave function. Within BCS theory one defines the pair wave function as[37]

$$\phi_k=\langle c_{-k\downarrow}c_{k\uparrow}\rangle=\frac{\Delta_k}{2E_k} , \tag{B10}$$

which obeys the Schrödinger-like equation:

$$2(\varepsilon_k-\mu)\phi_k=(1-2n_k)\left[-\frac{1}{N}\sum_{k'}V_{kk'}\phi_{k'}\right] . \tag{B11}$$

In the dilute limit, $E_k=E_b=2|\mu|$ and it is simple to obtain the pair wave function amplitude in real space

$$f(R-R')=\langle c_{R\uparrow}c_{R'\downarrow}\rangle \tag{B12}$$

by Fourier transforming Eq. (B10), using Eqs. (7) and (4) for the gap and kinetic energies:

$$f(R)\propto \left[c\delta_{R,0}+\tfrac{1}{4}(\delta_{R,\hat{x}}+\delta_{R,-\hat{x}}+\delta_{R,\hat{y}}+\delta_{R,-\hat{y}})\right.$$
$$\left.-\frac{1}{2}\left[c'+\frac{\rho}{2}\right](\delta_{R,\hat{z}}+\delta_{R,-\hat{z}})\right] \tag{B13}$$

The pair wave function is given by

$$|\psi\rangle=\sum_{RR'}f(R-R')c_{R\uparrow}^\dagger c_{R'\downarrow}^\dagger|0\rangle \tag{B14}$$

and we obtain

$$|\psi\rangle=\frac{1}{[c^2+\tfrac{1}{4}+\tfrac{1}{2}(c'+\rho/2)^2]^{1/2}}$$
$$\times\left[c|\psi_p\rangle+\tfrac{1}{2}|\psi_{xy}\rangle-\frac{c'+\rho/2}{\sqrt{2}}|\psi_z\rangle\right] . \tag{B15}$$

The reader can easily verify that the eigenvalue equation for H given in Eq. (B2) gives rise to the same ground-state wave function with c and c' given by Eq. (B9) and $E_b=-E_0$.

Equation (B15) clearly displays the meaning of the parameters c and c'. c gives the ratio of the doubly occupied piece of the wave function to the singlet component in the plane. In particular, as U increases c necessarily goes to zero. This is most clearly seen from the expression for c obtained from Eq. (B7a):

$$c=\frac{(k/4)(1+\rho^2/2)+(k\rho/4)c'}{E_b+U} . \tag{B16}$$

The parameter c' gives the deviation in the amplitude of

the pair wave function involving pairs in the z direction with respect to what would be obtained in the absence of anisotropy in the nearest-neighbor repulsion. Starting with a doubly occupied site, the hopping interaction will give a singlet pair in the z direction or in the xy plane with relative amplitudes given by the hopping anisotropy ρ. However, if the interaction V is anisotropic ($v \neq 1$) the pair amplitude in the z direction will be enhanced or suppressed according to whether $v < 1$ or $v > 1$, as seen from Eqs. (B9b) and (B15).

The coherence length in this limit

$$\xi^2 = \frac{\langle \psi | R^2 | \psi \rangle}{\langle \psi | \psi \rangle} \tag{B17}$$

follows immediately from the wave function amplitudes. In the plane we obtain:

$$\xi_x = \frac{1}{\sqrt{2}[1 + 4c^2 + \frac{1}{2}(\rho + 2c')^2]^{1/2}} \tag{B18}$$

and perpendicular to the planes

$$\xi_z = \frac{\rho + 2c'}{\sqrt{2}[1 + 4c^2 + \frac{1}{2}(\rho + 2c')^2]^{1/2}} . \tag{B19}$$

Note that for $v = 1$ we obtain simply:

$$\frac{\xi_z}{\xi_x} = \rho , \tag{B20}$$

which differs from the weak-coupling dilute limit behavior $\xi_z / \xi_x = \sqrt{\rho}$. The coherence lengths Eqs. (B18) and (B19) are smaller than one lattice spacing. In the limit of large U, $c \to 0$ and we obtain

$$\xi_x^2 + \xi_y^2 + \xi_z^2 = 1 \tag{B21}$$

as expected.

[1] Proceedings of the International Conference on Materials and Mechanisms of Superconductivity, High Temperature Superconductors II, Stanford, 1989, edited by R. N. Shelton, W. A. Harrison, and N. E. Phillips [Physica 162-164C, 1989], and references therein.

[2] J. E. Hirsch, Phys. Lett. A 134, 451 (1989); 136, 163 (1989); J. E. Hirsch and S. Tang, Phys. Rev. B 40, 2179 (1989).

[3] J. E. Hirsch, Physica C 158, 326 (1989); Phys. Lett. A 138, 83 (1989).

[4] J. E. Hirsch and F. Marsiglio, Phys. Rev. B 39, 11 515 (1989); 41, 2049 (1990).

[5] F. Marsiglio and J. E. Hirsch, in Proceedings of the International Conference on Materials and Mechanisims of Superconductivity, High Temperature Superconductors II, Stanford, 1989 (Ref. 1), p. 1451.

[6] J. B. Torrance et al., Phys. Rev. Lett. 61, 1127 (1988).

[7] N. Tanahashi et al., Jpn. J. Appl. Phys. 28, L762 (1989).

[8] H. Takagi et al., Phys. Rev. B 40, 2254 (1989).

[9] J. J. Neumeier et al., Phys. Rev. Lett. 63, 2516 (1989).

[10] P. W. Anderson, Science 235, 1196 (1987); J. R. Schrieffer et al., Phys. Rev. Lett. 60, 944 (1988); V. J. Emerg, ibid. 58, 3759 (1987); R. Laughlin, Science 242, 525 (1988); F. C. Zhang and T. M. Rice, Phys. Rev. B 37, 3759 (1988); Strong Correlation and Superconductivity, edited by H. Fukuyama, S. Maekawa, and A. P. Molozemoff (Springer, Berlin, 1989), and references therein.

[11] J. E. Hirsch, Physica 161C, 185 (1990); F. Marsiglio and J. E. Hirsch, ibid. 165C, 71 (1990).

[12] Y. Iye et al., Physica 153-155C, 26 (1988).

[13] T. K. Worthington et al., Physica 153-155C, 32 (1988).

[14] M. Sato, in Ref. 1, p. 38. Physica 153-155C, 38 (1988).

[15] D. R. Harshman et al., Phys. Rev. B 39, 851 (1989).

[16] G. A. Thomas et al., Phys. Rev. Lett. 61, 1313 (1988).

[17] R. Manzke, in Proceedings of the International Conference on Materials and Mechanisms of Superconductivity, High Temperature Superconductors II, Stanford, 1989 (Ref. 1), p. 1381.

[18] M. L. Wu et al., Phys. Rev. Lett. 58, 408 (1987).

[19] M. F. Crommie et al., Phys. Rev. B 39, 4231 (1989), and references therein.

[20] T. R. Lemberger et al., Phys. Rev. B 18, 6057 (1978).

[21] J. D. Jorgensen et al., Phys. Rev. B 36, 3608 (1987).

[22] See, for example, L. P. Gor'kov and N. B. Kopnin, Usp. Fiz. Nauk 156, 117 (1988) [Sov. Phys. Usp. 31(9), 850 (1989)].

[23] E. Helfand and N. R. Werthamer, Phys. Rev. 147, 288 (1966).

[24] D. H. Douglass, Jr. and L. M. Falicov, Progress in Low Temperature Physics, edited by C. J. Gorter (North-Holland, Amsterdam, 1964), Vol. 4, p. 97.

[25] J. E. Hirsch and F. Marsiglio, in Proceedings of the International Conference on Materials and Mechanisms of Superconductivity, High Temperature Superconductors II, Stanford, 1989 (Ref. 1), p. 591.

[26] M. Gurvitch et al., Phys. Rev. Lett. 63, 1008 (1989).

[27] R. Manzke et al., Europhys. Lett. 9, 477 (1989).

[28] F. Marsiglio and J. E. Hirsch, Physica 159C, 157 (1989).

[29] See, for example, G. Rickayzen, in Superconductivity, edited by R. D. Parks (Dekker, New York, 1969), Vol. 1, p. 51.

[30] See, for example, M. Takigawa et al., Phys. Rev. B 39, 7371 (1989).

[31] N. Bulut et al. (unpublished).

[32] The Hebel-Slichter peak is reported to be seen in M. Mehring, IBM J. Res. Dev. 33, 343 (1989), but is reported to be absent in P. C. Hammel et al., Phys. Rev. Lett. 63, 1992 (1989).

[33] J. Orenstein et al. (unpublished); T. Timusk and D. B. Tanner, in Physical Properties of High Temperature Superconductors I, edited by D. M. Ginsberg (World Scientific, New Jersey, 1989), p. 339.

[34] Y. J. Uemura et al., Phys. Rev. Lett. 62, 2317 (1989).

[35] Y. Tokura, H. Takagi, and S. Uchida, Nature 337, 345 (1989); Phys. Rev. Lett. 62, 1197 (1989).

[36] J. E. Hirsch and F. Marsiglio, Phys. Lett. A 140, 122 (1989).

[37] P. Nozieres and S. Schmitt-Rink, J. Low Temp. Phys. 59, 195 (1985).